Electronic Supplementary Information

for

Binuclear Iridium(III) Complexes for Efficient Near-Infrared Light-Emitting Electrochemical Cells with Electroluminescence up to 800 nm

Lavinia Ballerini,[a] Wei-Min Zhang,[b] Thomaz Groizard,[c] Christophe Gourlaouen,[c] Federico Polo,[d,e] Abdelaziz Jouaiti,[f,] Hai-Ching Su,[b,]* and Matteo Mauro[a,]**

[a] *Institut de Physique et Chimie des Matériaux de Strasbourg (IPCMS) UMR7504, Université de Strasbourg & CNRS, 23 rue du Loess, 67083 Strasbourg (France)*
E-mail: mauro@unistra.fr

[b] *Institute of Lighting and Energy Photonics, National Yang Ming Chiao Tung University, Tainan 71150, Taiwan*
E-mail: haichingsu@nycu.edu.tw

[c] *Laboratoire de Chimie Quantique, Institut de Chimie de Strasbourg UMR7177, Université de Strasbourg & CNRS, Rue Blaise Pascal, 67008 Strasbourg (France)*

[d] *Department of Molecular Sciences and Nanosystems, Ca' Foscari University of Venice Via Torino 155, 30172 Venezia (Italy)*

[e] *European Centre for Living Technology (ECLT), Ca' Bottacin, 30124, Venice, Italy*

[f] *Laboratoire de Synthèse et Fonctions des Architectures Moléculaires, UMR7140 Chimie de la Matiere Complexe, Université de Strasbourg & CNRS*
4 rue Blaise, Pascal 67000 Strasbourg (France)
E-mail: jouaiti@unistra.fr

Table of Contents

Experimental section

General consideration.

All procedures involving iridium complexes were carried out under an argon atmosphere using standard Schlenk techniques. Nuclear magnetic resonance spectra were recorded using a Bruker Avance III HD 500 MHz spectrometer equipped with a N_2 cryo-probe CPPBBO Prodigy at 298 K. ^{1}H and $^{13}C\{^{1}H\}$ NMR spectra were calibrated to residual solvent signals. HR-ESI-MS spectra were recorded on a MicroToF Bruker equipped with an electrospray ionization source. $IrCl_3 \times nH_2O$, 2-phenylpyridine, 5-chloropyrazine-2-carbaldehyde, (3,5-di-*tert*-butylphenyl)boronic acid, dithiooxamide, $Pd(PPh_3)_4$, 2-aminothiophenol, 5-(3,5-di-tert-butylphenyl)pyrazine-2-carbaldehyde, $AgPF_6$, KPF_6, poly(methyl methacrylate) (PMMA) beads (M_W = 35000), were purchased from Aldrich Chemicals, Acros or BLDPharm and used without further purification. The synthesis of **L1** and **L3** was carried out following previously reported procedures and the chemical analyses and reaction yields agrees well with the reported data.[S1]

Synthetic procedures.

Synthesis of 5-(3,5-di-tert-butylphenyl)pyrazine-2-carbaldehyde

A mixture of 5-chloropyrazine-2-carbaldehyde (1.0 g, 7.0 mmol), Na_2CO_3 (2.72 g, 25.6 mmol) and (3,5-di-tert-butylphenyl)boronic acid (2.12 g, 9.0 mmol) in 50 mL of a mixture 1,4-dioxane/H_2O (4:1 v/v) was degassed by steady bubbling with argon for 20 minutes. $Pd(PPh_3)_4$ (0.02 g, 0.018 mmol) was added and the mixture was refluxed 8 hours under argon. After cooling, the mixture was extracted with CH_2Cl_2 (3×40 mL). The combined organic layers were washed with brine, dried over $MgSO_4$ and evaporated under vacuum. The residue was purified by silica gel column chromatography with petroleum ether/CH_2Cl_2 mixture varying from 100:0 to 50:50 as eluent to provide the target compound as white solid (2.0 g, yield 96%). ^{1}H NMR ($CDCl_3$, 300 MHz) δ: 10.21 (s, 1H), 9.23 (d, J = 1.2 Hz, 1H), 9.18 (d, J = 1.2 Hz, 1H), 7.96 (d,

J = 1.8 Hz, 2H), 7.66 (t, *J* = 1.8 Hz, 1H), 1.48 (s, 18H). ^{13}C NMR ($CDCl_3$, 125 MHz) δ: 192.3, 157.1, 152.0, 144.8, 143.0, 142.1, 134.7, 125.6, 122.0, 35.1, 31.4. HR-MS (ESI): m/*z* $[M + H]^+$ calcd for $C_{19}H_{25}N_2O$ 297.1889, found 297.1954.

Synthesis of 2-(5-(3,5-di-tert-butylphenyl)pyrazin-2-yl)benzo[d]thiazole (L2)

Two drops of glacial acetic acid were added to a mixture of 2-aminothiophenol (0.2 mL, 1.8 mmol) and 5-(3,5-di-tert-butylphenyl)pyrazine-2-carbaldehyde (0.55 g, 1.8 mmol) in ethanol (15 mL). The reaction mixture was refluxed with stirring for 7 hours. The precipitate formed after cooling was filtered off washed with MeOH and dried in air to provide the target compound **L2** as white solid (0.5 g, yield 53%). ^{1}H NMR ($CDCl_3$, 300 MHz) δ: 9.65 (s, 1H), 9.09 (s, 1H),-8.18 (d, *J* = 5 Hz, 1H),-8.02 (d, *J* = 5 Hz, 1H), 7.95 (d, *J* = 2.25 Hz, 2H), 7.63 (t, *J* = 5 Hz, 1H), 7.57 (td, *J* = 2.25 Hz, *J* = 5 Hz, 1H), 7.48 (td, *J* = 2.25 Hz, *J* = 5 Hz, 1H), 1.45 (s, 18H). ^{13}C NMR ($CDCl_3$, 125 MHz) δ: 166.9, 154.8, 154.4, 151.8, 144.5, 141.5, 141.4, 135.9, 135.3, 126.5, 126.0, 124.8, 123.8, 122.0, 121.6, 35.1, 31.5. HR-MS (ESI): m/*z* $[M + H]^+$ calcd for $C_{25}H_{28}N_3S$ 402.5720, found 402.1990.

Synthesis of ligand L4.

Compound **L4** was prepared by a synthetic procedure similar to that previously employed by us for obtaining ligand **L3**[37] except for using the corresponding carbaldehyde 5-(3,5-di-*tert*-butylphenyl)pyrazine-2-carbaldehyde. Yield 86%. ^{1}H NMR ($CDCl_3$, 500 MHz) δ: 9.48 (s, 2 H); 9.02 (s, 2 H); 7.90 (d, *J* = 2 Hz, 4 H); 7.59 (t, *J* = 2 Hz, 2 H); 1.40 (s, 36 H). ^{13}C NMR ($CDCl_3$, 125 MHz) δ: 168.8, 154.6, 153.9, 151.9, 144.4, 141.5, 140.7, 135.2, 124.9, 121.5, 35.1, 31.5. HR-MS (ESI): m/z $[M + H]^+$ calcd for $C_{40}H_{47}N_6S_2$, $[M + H]^+$ 675.3298, found 675.3290.

Synthesis of mononuclear complexes Ir-M1 and Ir-M2.

To a one-neck round-bottom flask the starting dimer $[Ir(ppy)_2Cl]_2$ (250.0 mg, 0.233 mmol, 1 equiv.) was stirred overnight in 30 ml of MeOH in the dark at room temperature with $AgPF_6$

(130.0 mg, 0.513 mmol, 2.2 equiv.). The AgCl formed was removed by filtration on Celite, and the resulting the *bis*-solvento complex was dried under reduced pressure and used without further purification for the second step. The solvato complex was reacted with two equiv. of ligand either **L1** or **L2** (187 mg, 0.466 mmol for **L1**, 187 mg, 0.466 mmol for **L2**) in 40 mL of a CH_2Cl_2/MeOH (1:1) mixture, and the latter was refluxed (55 °C) overnight. The crude was dried under reduced pressure and purified with silica gel chromatographic column using as eluent CH_2Cl_2/hexane (7:3) to CH_2Cl_2/MeOH (9:1). The pure fractions were than solubilized in 5 mL of CH_2Cl_2/MeOH (1:1) and the target complex precipitated with an aqueous saturated solution of KPF_6 and the obtained solid were washed with water (70 mL) and hexane (100 mL).

Complex Ir-M1: Light orange powder, 398 mg, 0.380 mmol (yield 82%). ^{1}H NMR (500 MHz, CD_2Cl_2) δ: 8.48 (d, *J* = 8.3 Hz, 1H), 8.41 (dd, *J* = 8.2, 1.4 Hz, 1H), 8.22 (s, 1H), 8.09 (d, *J* = 8.1 Hz, 1H), 8.00 (d, *J* = 8.1 Hz, 1H), 7.94 (d, *J* = 8.1 Hz, 1H), 7.85 – 7.74 (m, 4H), 7.69 (d, *J* = 5.5 Hz, 1H), 7.55 (dd, *J* = 11.7, 4.2 Hz, 3H), 7.26 (t, *J* = 7.7 Hz, 1H), 7.22 – 7.09 (m, 4H), 7.00 (dt, *J* = 16.0, 9.1 Hz, 5H), 6.46 (d, *J* = 7.5 Hz, 1H), 6.31 (d, *J* = 7.5 Hz, 1H), 1.31 (s, 18H). ^{13}C{^{1}H} NMR (126 MHz, CD_2Cl_2) d: 169.9, 168.5, 167.8, 153.1, 151.2, 150.4, 150.1, 149.6, 149.2, 148.0, 147.7, 144.8, 144.3, 143.2, 139.0, 138.8, 137.3, 134.8, 133.9, 132.9, 131.8, 131.5, 131.1, 129.3, 128.8, 126.8, 125.5, 125.5, 125.1, 124.3, 124.0, 124.0, 123.7, 123.4, 123.1, 121.9, 120.6, 120.2, 35.6, 31.6. HR-ESI-MS: calcd. for $[C_{48}H_{44}IrN_4S]^+$ 901.2910 m/*z*; found for ($[M]^+$) 901.2916 m/*z*.

Complex Ir-M2: Dark red powder, 393 mg, 0.375 mmol (yield 81%). ^{1}H NMR (500 MHz, CD_2Cl_2) δ: 9.60 (s, 1H), 8.33 (s, 1H), 8.13 (d, *J* = 8.2 Hz, 1H), 8.00 (d, *J* = 8.1 Hz, 1H), 7.96 (d, *J* = 8.1 Hz, 1H), 7.88 – 7.76 (m, 4H), 7.68 – 7.61 (m, 4H), 7.61 – 7.55 (m, 2H), 7.29 (t, *J* = 7.7 Hz, 1H), 7.18 (t, *J* = 7.5 Hz, 2H), 7.10 – 6.98 (m, 5H), 6.44 (d, *J* = 7.5 Hz, 1H), 6.33 (d, *J* = 7.5 Hz, 1H), 1.32 (s, 18H). ^{13}C{^{1}H} NMR (126 MHz, CD_2Cl_2) d: 168.2, 167.6, 167.1, 159.0, 153.0, 151.0, 150.5, 149.3, 147.1, 146.6, 146.5, 144.8, 144.5, 144.4, 141.6, 139.4, 139.2, 135.0,

133.1, 132.7, 131.9, 131.7, 131.2, 129.6, 129.3, 127.7, 125.6, 125.6, 124.7, 124.5, 124.2, 123.9, 123.8, 123.1, 122.5, 120.8, 120.4, 35.6, 31.6. HR-ESI-MS: calcd. for $[C_{47}H_{43}IrN_5S]^+$ 902.2863 m/*z*; found for ($[M]^+$) 902.2878 m/*z*.

Synthesis of binuclear complexes Ir-D1 and Ir-D2.

To a one-neck round-bottom flask the starting dimer $[Ir(ppy)_2Cl]_2$ (500.0 mg, 0.466 mmol, 1 equiv.) was stirred overnight in 30 ml of MeOH in the dark at room temperature with $AgPF_6$ (259 mg, 1.026 mmol, 2.2 equiv.). The AgCl formed was removed by filtration on Celite, and the resulting the *bis*-solvento complex was dried under reduced pressure and used without further purification for the second step. The solvato complex was reacted with one equiv. of ligand either **L3** or **L4** (314 mg, 0.466 mmol for **L3**, 315 mg, 0.466 mmol for **L4**) in 56 mL of a CH_2Cl_2/MeOH (1:1) mixture, and the latter was refluxed (55 °C) overnight. The crude was dried under reduced pressure and purified with silica gel chromatographic column using as eluent CH_2Cl_2/hexane (4:6) to CH_2Cl_2. The pure fractions were than solubilized in 5 mL of CH_2Cl_2/MeOH (2:8) and the target complex precipitated with an aqueous saturated solution of KPF_6 and the obtained solid were washed with water (70 mL) and hexane (100 mL).

Complex Ir-D1: Brown powder, 448 mg, 0.228 mmol (yield 49%). ^{1}H NMR (500 MHz, CD_2Cl_2) δ: 8.32–8.25 (m, 6H), 8.21 (d, 2H), 8.17 (d, *J* = 1.2 Hz, 4H), 8.05 (d, *J* = 5.6 Hz, 4H), 8.03 (d, *J* = 8.2 Hz, 2H), 7.94 (ddt, *J* = 25.7, 15.9, 5.6 Hz, 20H), 7.86 – 7.73 (m, 20H), 7.71 (d, *J* = 5.6 Hz, 2H), 7.55 (d, *J* = 5.6 Hz, 4H), 7.52 (d, *J* = 1.3 Hz, 7H), 7.33 (dt, *J* = 22.0, 7.0 Hz, 10H), 7.15 (t, *J* = 7.1 Hz, 17H), 7.10 (dd, *J* = 15.7, 7.9 Hz, 8H), 7.01 (d, *J* = 6.6 Hz, 6H), 6.95 (dd, *J* = 16.2, 8.3 Hz, 5H), 6.67 (d, *J* = 7.5 Hz, 4H), 6.54 (d, *J* = 7.5 Hz, 2H), 6.29 (d, *J* = 7.5 Hz, 2H), 6.21 (d, *J* = 7.5 Hz, 4H), 1.29 (s, 108H). ^{13}C{^{1}H} NMR (126 MHz, CD_2Cl_2) d: 173.3, 173.2, 168.2, 167.8, 167.5, 167.0, 153.1, 153.0, 151.8, 150.3, 150.2, 150.0, 149.9, 149.8, 149.1, 148.9, 147.8, 147.4, 146.0, 145.7, 145.5, 145.2, 144.6, 144.4, 143.8, 143.6, 139.4, 139.3, 139.2, 139.1, 137.1, 137.0, 134.5, 134.1, 133.8, 133.7, 131.9, 131.8, 131.4, 131.3, 131.2, 125.9, 125.7,

125.6, 125.4, 125.4, 125.3, 125.2, 125.2, 124.9, 124.7, 124.6, 124.6, 124.3, 124.1, 124.0, 122.00, 122.0, 120.7, 120.6, 120.3, 120.0, 35.5, 31.6. HR-ESI-MS: calcd. for $[C_{86}H_{80}F_6Ir_2N_8PS_2]^+$ 1819.4842 m/*z*; found for ($[M]^+$) 1819.4881 m/*z*.

Complex Ir-D2: Dark green powder, 486 mg, 0.247 mmol (yield 53%). ^{1}H NMR (500 MHz, CD_2Cl_2) δ: 9.22 (s, 5H), 8.30 (d, *J* = 0.9 Hz, 2H), 8.27 (d, *J* = 0.9 Hz, 4H), 8.08 – 8.01 (m, 6H), 7.99 – 7.88 (m, 14H), 7.88 – 7.76 (m, 21H), 7.72 (d, *J* = 5.7 Hz, 2H), 7.66 – 7.59 (m, 17H), 7.57 (d, *J* = 5.7 Hz, 4H), 7.52 (d, *J* = 5.6 Hz, 2H), 7.39 – 7.29 (m, 10H), 7.21 – 7.12 (m, 14H), 7.08 – 6.98 (m, *J* = 14.9, 6.7 Hz, 12H), 6.66 (d, *J* = 7.5 Hz, 4H), 6.56 (d, *J* = 7.5 Hz, 2H), 6.33 (d, *J* = 7.5 Hz, 2H), 6.26 (d, *J* = 7.5 Hz, 4H), 1.31 (s, 108H). ^{13}C{^{1}H} NMR (126 MHz, CD_2Cl_2) d: 171.2, 171.1, 167.9, 167.4, 167.2, 166.7, 159.3, 159.2, 153.0, 152.9, 152.1, 150.8, 150.7, 150.7, 150.6, 150.1, 146.5, 146.1, 145.8, 145.5, 145.0, 144.7, 144.6, 144.5, 143.9, 143.8, 141.7, 141.7, 139.6, 139.5, 139.4, 139.4, 134.3, 134.0, 133.1, 133.0, 132.0, 132.0, 131.5, 131.5, 131.4, 131.3, 127.9, 127.9, 126.1, 125.9, 125.8, 125.4, 125.3, 125.2, 125.1, 125.0, 124.5, 124.5, 124.4, 122.6, 122.5, 120.8, 120.8, 120.5, 120.2, 35.6, 31.5. HR-ESI-MS calcd. for $[C_{84}H_{78}F_6Ir_2N_{10}PS_2]^+$ 1821.4747 m/*z*; found for ($[M]^+$) 1821.4711 m/*z*.

Photophysical measurements

Instrument details. Absorption spectra were recorded using a Perkin Elmer Lambda 950 double-beam UV-VIS spectrophotometer and baseline corrected. Steady-state emission spectra were recorded on a Horiba Jobin−Yvon IBH FL-322 Fluorolog 3 spectrometer equipped with a 450 W xenon arc lamp, double-grating excitation, and emission monochromators (2.1 nm mm^{-1} of dispersion; 1200 grooves mm^{-1}) and a Hamamatsu R13456 red sensitive Peltier-cooled PMT detector. Emission and excitation spectra were corrected for source intensity (lamp and grating) and emission spectral response (detector and grating) by standard correction curves. Time-resolved measurements were performed using either the Time-Correlated Single-Photon Counting (TCSPC) or the Multi-Channel Scaling (MCS) electronics option of the

TimeHarp 260 board installed on a PicoQuant FluoTime 300 fluorimeter (PicoQuant GmbH, Germany), equipped with a PDL 820 laser pulse driver. A pulsed laser diode LDH-P-C-375 (λ = 375 nm, pulse full width at half maximum <50 ps, repetition rate 200 kHz–40 MHz) was used to excite the sample and mounted directly on the sample chamber at 90°. The photons were collected by a PMA Hybrid-07 single photon counting detector. The data were acquired by using the commercially available software EasyTau II (PicoQuant GmbH, Germany), while data analysis was performed using the built-in software FluoFit (PicoQuant GmbH, Germany).

All the solvents were spectrophotometric grade. Dearated samples were prepared by the freeze–pump–thaw technique by using a home-made quartz cuvette equipped with a Rotaflo stopcock. Luminescence quantum yields were measured in optically dilute solutions (optical density <0.1 at the excitation wavelength) and compared to reference emitter by following the method of Demas and Crosby.[S2] The $Ru(bpy)_3Cl_2$ complex in air-equilibrated water solution at room temperature was used as reference (PLQY = 0.04).[S3] Solid state PLQY values were recorded at a fixed excitation wavelength by using a Hamamatsu Photonics absolute PLQY measurements system Quantaurus QY equipped with CW Xenon light source (150 W), monochromator, integrating sphere, C7473 photonics multi-channel analyzer and employing the commercially available U6039-05 PLQY measurement software (Hamamatsu Photonics Ltd., Shizuoka, Japan). All measurements were repeated five times at the excitation wavelength λ_{exc} = 400-425 nm, unless otherwise stated.

Methods. For time resolved measurements, data fitting was performed by employing the maximum likelihood estimation (MLE) methods and the quality of the fit was assessed by inspection of the reduced χ^2 function and of the weighted residuals. For multi-exponential decays, the intensity, namely I*(t)*, has been assumed to decay as the sum of individual single exponential decays (Eqn. 4):

$$I(t) = \sum_{i=1}^{n} \alpha_i exp\left(-\frac{t}{\tau_i}\right) \qquad \text{eqn. 4}$$

where τ_i are the decay times and α_i are the amplitude of the component at $t = 0$. In the tables, the percentages to the pre-exponential factors, α_i, are listed upon normalization.

Intensity average lifetimes were calculated by using the following equation (Eqn. 5):[S4]

$$\bar{\tau} = \frac{a_1\tau_1^2 + a_2\tau_2^2}{a_1\tau_1 + a_2\tau_2} \qquad \text{eqn. 5}$$

Electrochemical characterization

The electrochemical properties of the complexes were assessed by means of cyclic voltammetry (CV). The CV experiments were carried out using a three-neck electrochemical cell in anhydrous and degassed dichloromethane/0.1M $TBAPF_6$ solution under an Ar atmosphere, using a 1 mM concentration for the iridium compound. Tetra-n-butylammonium hexafluorophosphate ($TBAPF_6$, BLDpharm, 97%) was used at the supporting electrolyte and employed as received. The working electrode was a glassy-carbon (GC) disk electrode (3 mm diameter, BASMF2012 Sigma-Aldrich). The electrode was polished as already described elsewhere.[S5] Before experiments, the electrode was further polished with a 0.05 mm polycrystalline diamond suspension (Buehler, MetaDi) and electrochemically activated in the background solution by means of several voltammetric cycles at 0.5 Vs^{-1} between the anodic and the cathodic solvent/electrolyte discharges, until the expected quality features were attained.[S6] One platinum wire served as the counter electrode and a silver wire was used as a quasi-reference electrode. At the end of each experiment, its potential was calibrated against the ferricenium/ferrocene couple, used as an internal redox standard. The solvent level was frequently checked and rinsed when necessary to avoid any change in the analyte concentration. A PalmSens4 potentiostat (PalmSens BV) was used for the CV experiments. The CV were blank-subtracted The effect of the scan rate was investigated over the range 50–500 mV s^{-1}, and the peak current was found to depend linearly on the square root of scan rate

for all compound, thus witnessing that the heterogeneous electron transfer process is diffusion-controlled. It is also worth noting that the peak-to-peak separation for all compound is in the range 90-120 mV (see Table 1 of the main text), which is larger than 59 mV expected for an ideal Nernstian behavior.[S5] However, the behavior of the redox couple ferrocene/ferricenium ($Fc^+|Fc^0$), used as internal standard, showed the same trend. This effect can be attributed to the ohmic drop of the system, which could not be properly controlled by potentiostat.

Despite the concentrations of all compounds, including Fc, were 1 mM, the current intensities of the CVs of **Ir-D1** and **Ir-D2** for the $R_{1\text{-}2,i}$ processes appeared to be lower than those of the mononuclear counterparts by a factor of 1.8. This is in line with the square root of the ratio of the diffusion coefficients of Fc (1.13×10^{-5} cm^2 s^{-1} in DMF/0.1 M TBAP)[S6] and the investigated mononuclear (**Ir-M1** and **Ir-M2**) and binuclear (**Ir-D1** and **Ir-D2**) complexes, which we estimated to be *ca.* 9×10^{-6} and 3×10^{-6} cm^2 s^{-1}, respectively, by the CV of the $R_{1,i}$ processes knowing the area of the electrode.[46] Whereas the behavior of $O_{1,i}$ processes for **Ir-D1** and **Ir-D2** is more complicated as it involves the simultaneous oxidation of two Ir metal centers. For such a process, a bielectronic wave is expected for two identical non-interacting moieties connected by a bridge, which should lead to a distinctive peak-to-peak separation of 29 mV and a current intensity that almost double that of the monoelectronic counterpart. However, although the oxidation process is indeed bielectronic, it is not possible to observe the features described above, because the two metal centers interact (although poorly) with each other. This is a well-known behavior, described in literature, which involves thermodynamic and statistical effects.[S5,S6] Moreover, to these effects, one should also take into account the square root of the diffusion coefficient ratio and the fact that a proper compensation of the ohmic drop could not be attained.

Computational details

All calculation were made using the ADF-2019 code at the density functional theory with B3LYP functional (DFT).[S7] All atoms were described with the TZP basis-set. Scalar relativistic were introduced through the zero-order relativistic approximation (ZORA) Hamiltonian.[S8–S10] All calculations were made with a non-explicit dichloromethane solvent within the Conductor-like-screening model (COSMO).[S11] Weak interactions were introduced through Grimme D3 corrections.[S12] The structures of complexes **Ir-M1**, **Ir-M2**, **Ir-D1** and **Ir-D2** were fully optimized and the absorption spectra computed through time dependent DFT (TD-DFT) using the Tamm-Dancoff approximation (TDA).[S13] 40 roots were computed for the mononuclear complexes and 25 roots for the binuclear counterparts. Spin-orbit coupling corrections were introduced by perturbation of the computed spectra. Emission properties were determined after the optimization of excited states geometries through the TD-DFT approach, in the same conditions. The nature of the excited states has been analyzed with TheoDORE software.[S14]The electron density differences were computed using the dgrid package and visualized using ChimeraX software.[S15]

Averaged radiative rate constant values, $k_{r,ave}$, were estimated by using the following equation (eqn. 6)

$$k_{r,\,ave} = \frac{k_r^{T1,I} + k_r^{T1,II} e^{-\frac{\Delta E_{I,II}}{RT}} + k_r^{T1,III} e^{-\frac{\Delta E_{I,III}}{RT}}}{1 + e^{-\frac{\Delta E_{I,II}}{RT}} + e^{-\frac{\Delta E_{I,III}}{RT}}} \qquad \text{(eqn.6)}$$

where $k_r^{T1,I}$, $k_r^{T1,II}$ and $k_r^{T1,III}$ are the radiative rate contants computed for the T_1 sublevel ($T_{1,I}$, $T_{1,II}$, $T_{1,III}$), respectively, R is the ideal gaz constant and T is the absolute temperature (T = 293 K).

LEC device fabrication and characterization

For device fabrication, standard clean and UV/ozone treatment were performed on the indium-tin oxide (ITO) coated glass substrates. After cleaning, the substrates were spin-coated with a

poly(3,4-ethylenedioxythiophene):poly(styrene sulfonate) (PEDOT:PSS) layer (40 nm) at 3500 rpm and they were then baked at 150 °C for 30 min in ambient air. The mixture of complex (**Ir-M1**, **Ir-M2**, **Ir-D1** and **Ir-D2**) (80 wt.%) and 1-butyl-3-methylimidazolium hexafluorophosphate [$BMIMPF_6$] (20 wt.%) in acetonitrile solution was spun on top of the PEDOT:PSS layer. The ionic liquid [$BMIMPF_6$] was added to provide additional mobile ions to accelerate the device response. Various solution concentrations (40, 60, 80, or 100 mg mL^{-1}) were utilized in spin coating to deposit different emissive-layer thicknesses for device performance optimization. Spin coating of all emissive layers was performed at 2000 rpm in ambient air. The thicknesses of the emissive layers were measured by ellipsometry. After depositing the emissive layers, the samples were baked at 60 °C for 8 hours in a vacuum oven to remove the residual solvent. Finally, a silver top contact was deposited by thermal evaporation in a vacuum chamber (*ca.* 10^{-6} torr). The EL emission properties of these LECs were measured using source-measurement units (B2901A, Keysight) and a calibrated Si photodiode. The EL spectra of these LECs were acquired with a calibrated fiber-optic spectrometer (USB2000, Ocean Optics). All LEC devices were measured under constant bias voltages. Device measurements were performed in a nitrogen glove box to reduce the device degradation rate.

X-ray crystallographic analysis

The crystals were placed in oil, and a single crystal was selected, mounted on a glass fibre and placed in a low-temperature N_2 stream. X-ray diffraction data collection was carried out on a Bruker APEX II DUO Kappa-CCD diffractometer equipped with an Oxford Cryosystem liquid N_2 device, using Mo-Kα radiation (λ = 0.71073 Å). The crystal-detector distance was 38mm. The cell parameters were determined (APEX3 software)[S16] from reflections taken from three sets of 6 frames, each at 10 s exposure. The structure was solved using the program SHELXT-2014.[S17]The refinement and all further calculations were carried out using SHELXL-2018.[S18]

The H-atoms were included in calculated positions and treated as riding atoms using SHELXL default parameters. The non-H atoms were refined anisotropically, using weighted full-matrix least-squares on F^2. A semi-empirical absorption correction was applied using SADABS in APEX3.[S19] The SQUEEZE instruction in PLATON[S20] was applied. The residual electron density was assigned to 0.5 molecule of the dichloromethane solvent for compounds **IrM1** and **IrM2**. For this latter the PF_6 anion is disordered over two positions and the atoms C20 C21 and C22 are disordered over two positions.

For compounds **Ir-D2**, X-ray diffraction data collection was carried out on a Bruker PHOTON III DUO CPAD diffractometer equipped with an Oxford Cryosystem liquid N_2 device, using Mo-Kα radiation (λ = 0.71073 Å). The crystal-detector distance was 38mm. The cell parameters were determined (APEX3 software)[S16] from reflections taken from 1 set of 180 frames at 1s exposure. The structure was solved using the program SHELXT-2018.[S17] The refinement and all further calculations were carried out using SHELXL-2018.[S18] The H-atoms were included in calculated positions and treated as riding atoms using SHELXL default parameters. The non-H atoms were refined anisotropically, using weighted full-matrix least-squares on F2. A semi-empirical absorption correction was applied using SADABS in APEX3.[S19] The SQUEEZE instruction in PLATON[S20]was applied. The residual electron density was assigned to 0.75 molecule of the dichloromethane solvent, for compounds **Ir-D2**. For compounds **Ir-D1**, The atoms Cl5 is disordered over two positions.

CCDC 2338499–2338502 contains the supplementary crystallographic data for this paper. These data can be obtained free of charge from The Cambridge Crystallographic Data Centre via www.ccdc.cam.ac.uk/data_request/cif.

Thermal analysis

Thermogravimetric analyses were carried out on a Q50 systems from TA Instruments under air with a thermal scanning rate of 5°C min^{-1}.

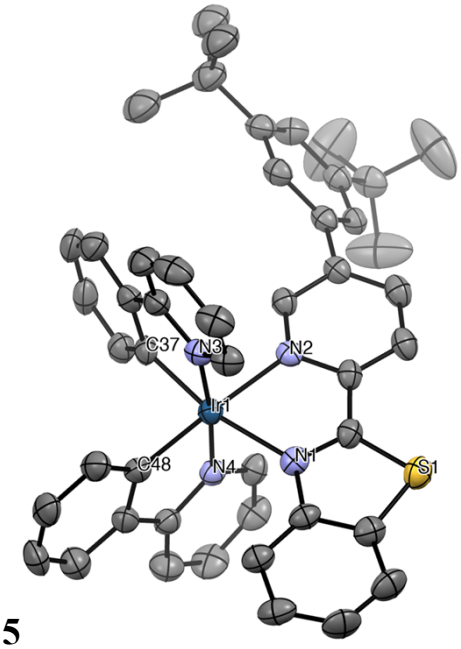

5

Figure S1. ORTEP diagram of compound **Ir-M1** with thermal ellipsoids shown at 50% probability level obtained by single-crystal X-ray diffractometric analysis. Hydrogen atoms, PF_6^- counter-anion and solvent molecules are omitted for clarity.

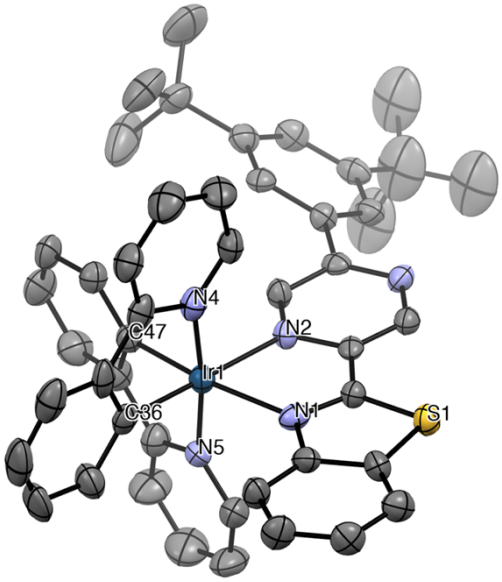

Figure S2. ORTEP diagram of compound **Ir-M2** with thermal ellipsoids shown at 50% probability level obtained by single-crystal X-ray diffractometric analysis. Hydrogen atoms, PF_6^- counter-anion and solvent molecules are omitted for clarity.

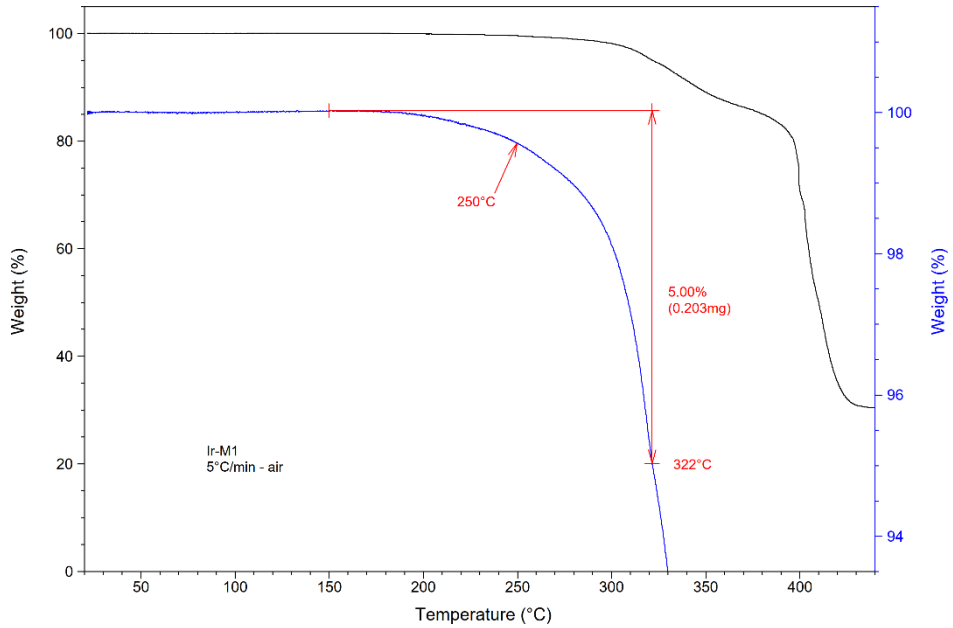

Figure S3. Thermogravimetric analysis (TGA) curve recorded for compound **Ir-M1** at heating rate of 5°C min^{-1} under air.

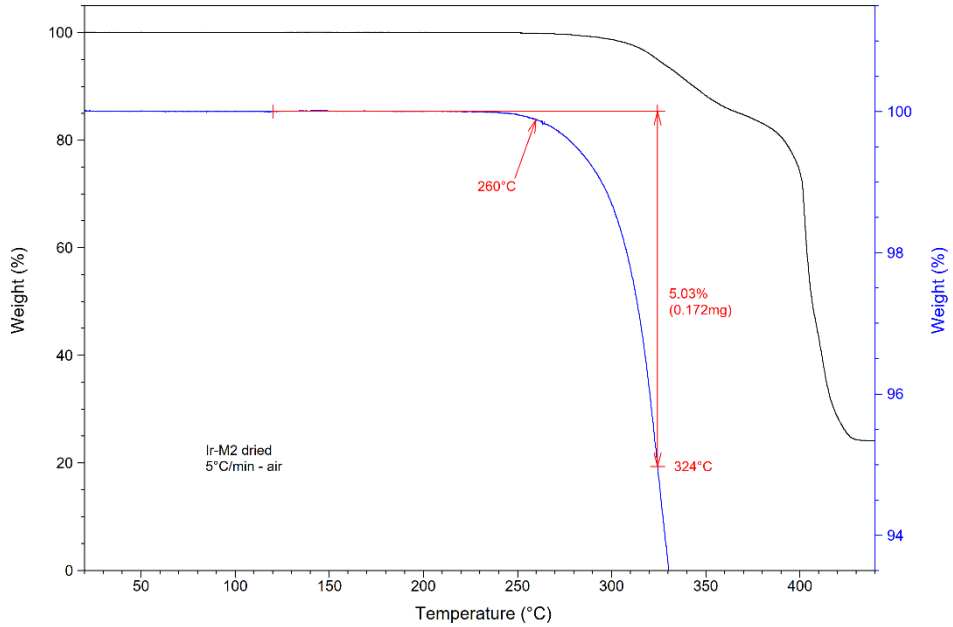

Figure S4. Thermogravimetric analysis (TGA) curve recorded for compound **Ir-M2** at heating rate of 5°C min^{-1} under air.

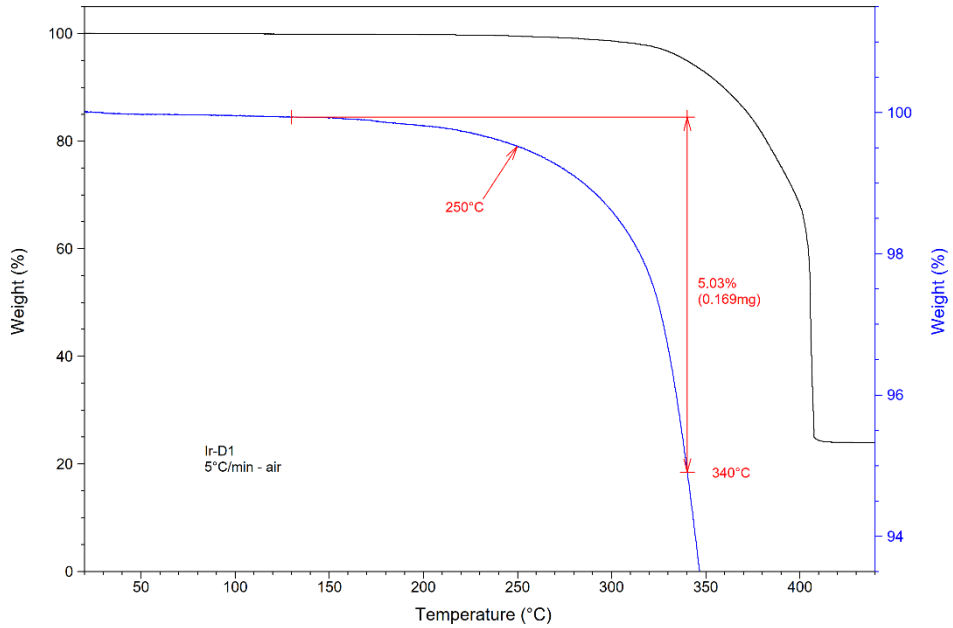

Figure S5. Thermogravimetric analysis (TGA) curve recorded for compound **Ir-D1** at heating rate of 5°C min^{-1} under air.

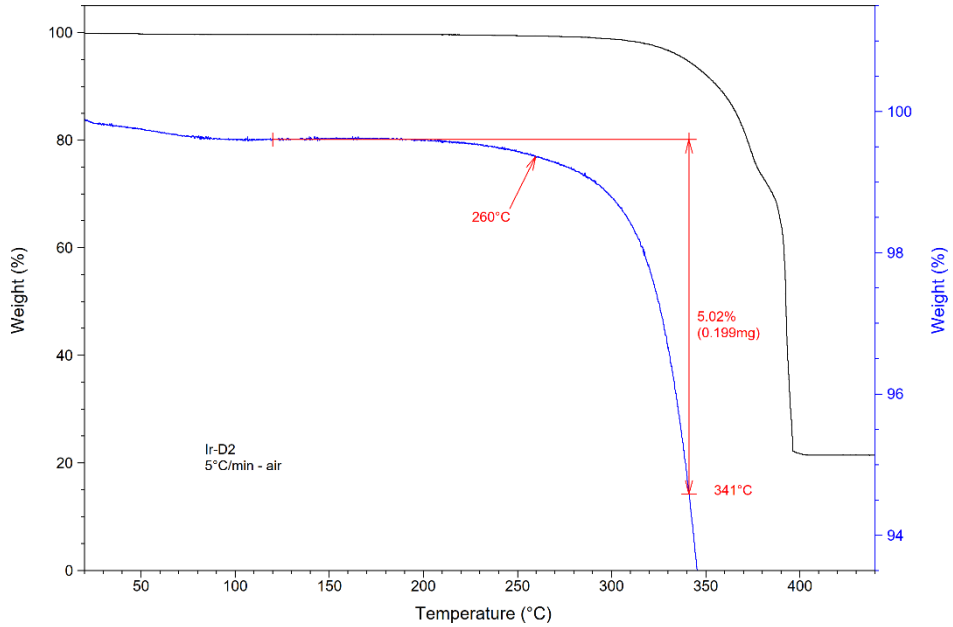

Figure S6. Thermogravimetric analysis (TGA) curve recorded for compound **Ir-Ds** at heating rate of 5°C min^{-1} under air.

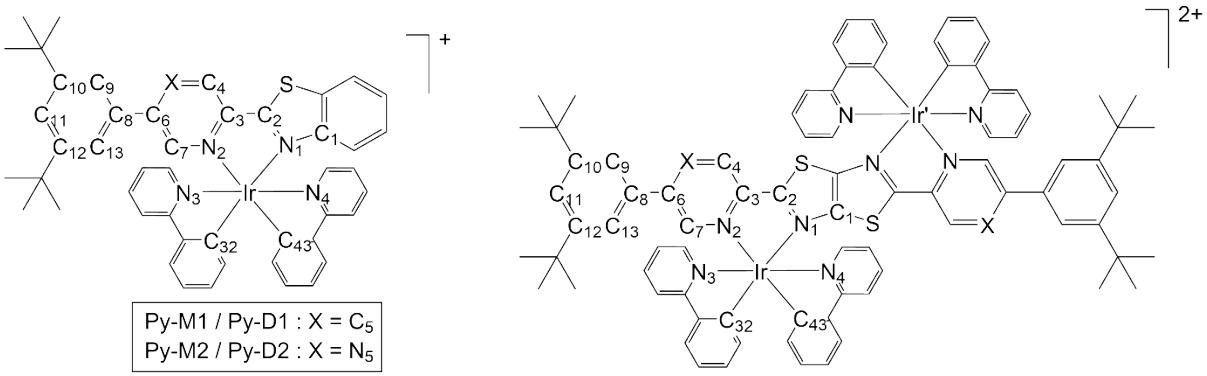

Figure S7. Atom labelling employed for the mononuclear (*left*) and dinuclear (right) complexes.

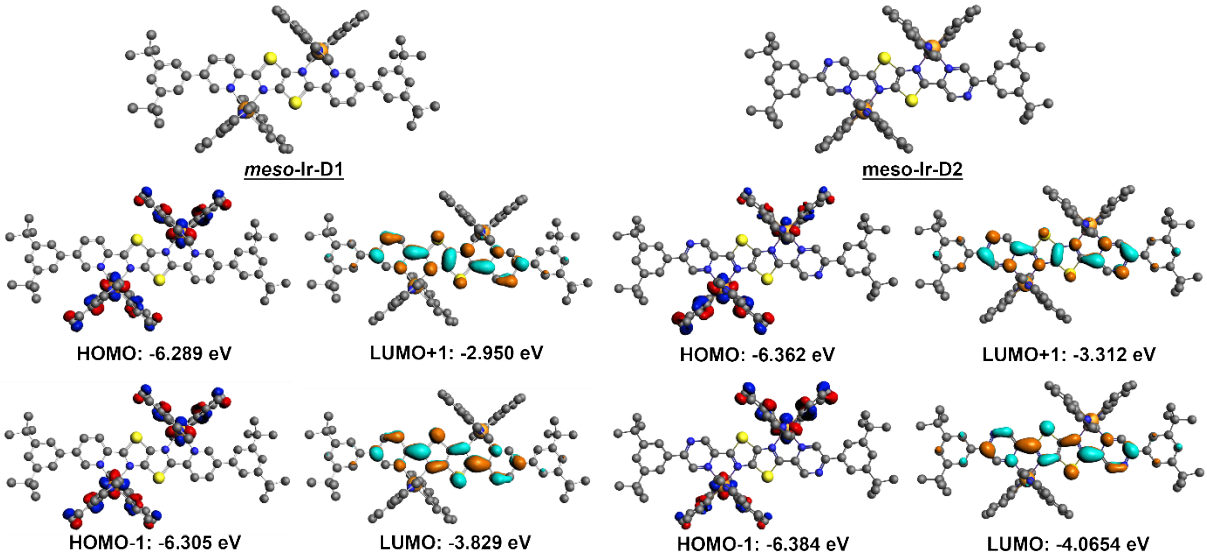

Figure S8. Frontier orbitals of ***meso*-Ir-D1** and ***meso*-Ir-D2**. Ir atoms are orange, S atoms are yellow, N atoms are blue and C atoms are grey. H atoms were eluded for visibility.

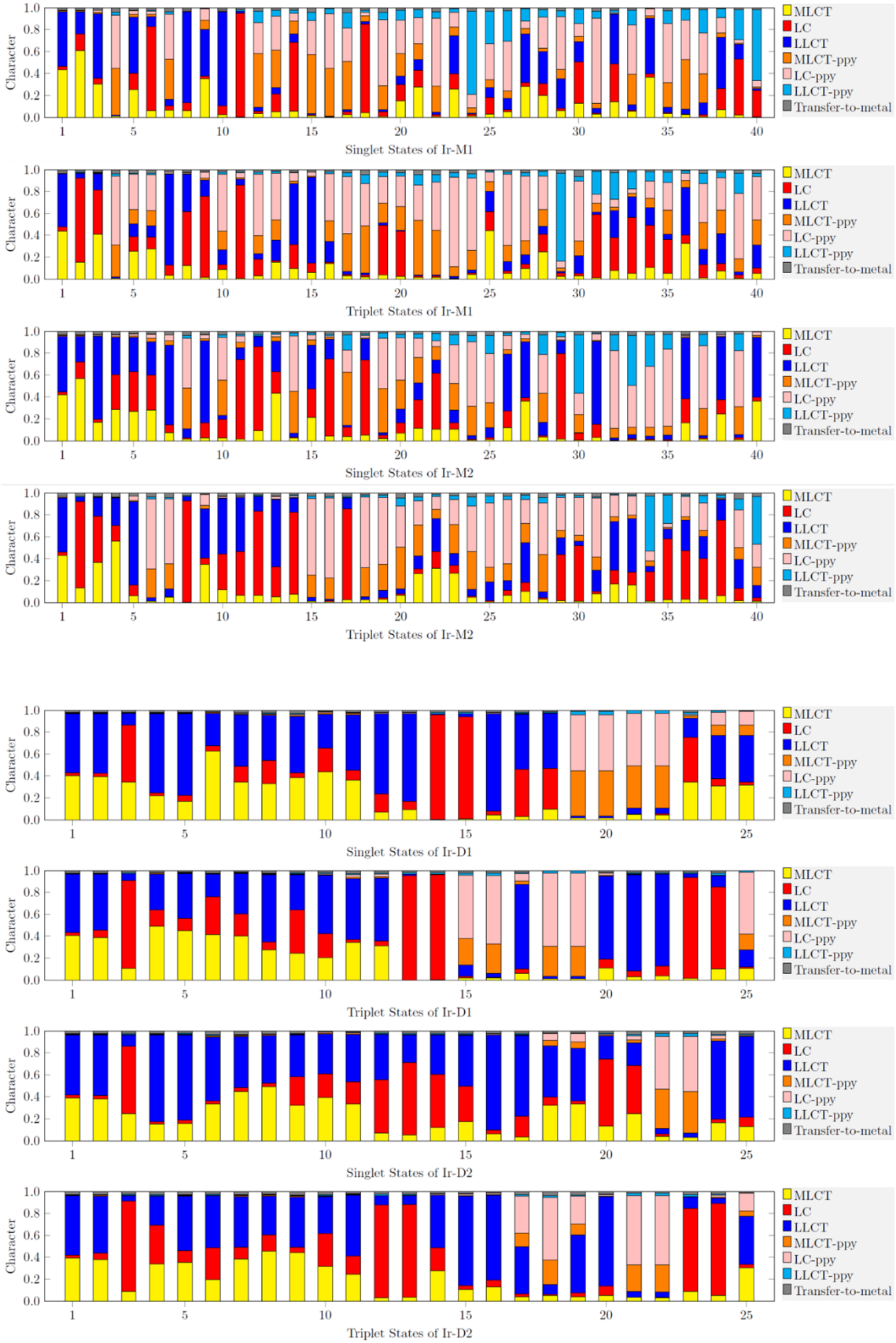

Figure S9. TheoDORE analysis of the singlet and triplet excited states computed for mononuclear **Ir-M1** and **Ir-M2** and binuclear **Ir-D1** and **Ir-D2** derivatives.

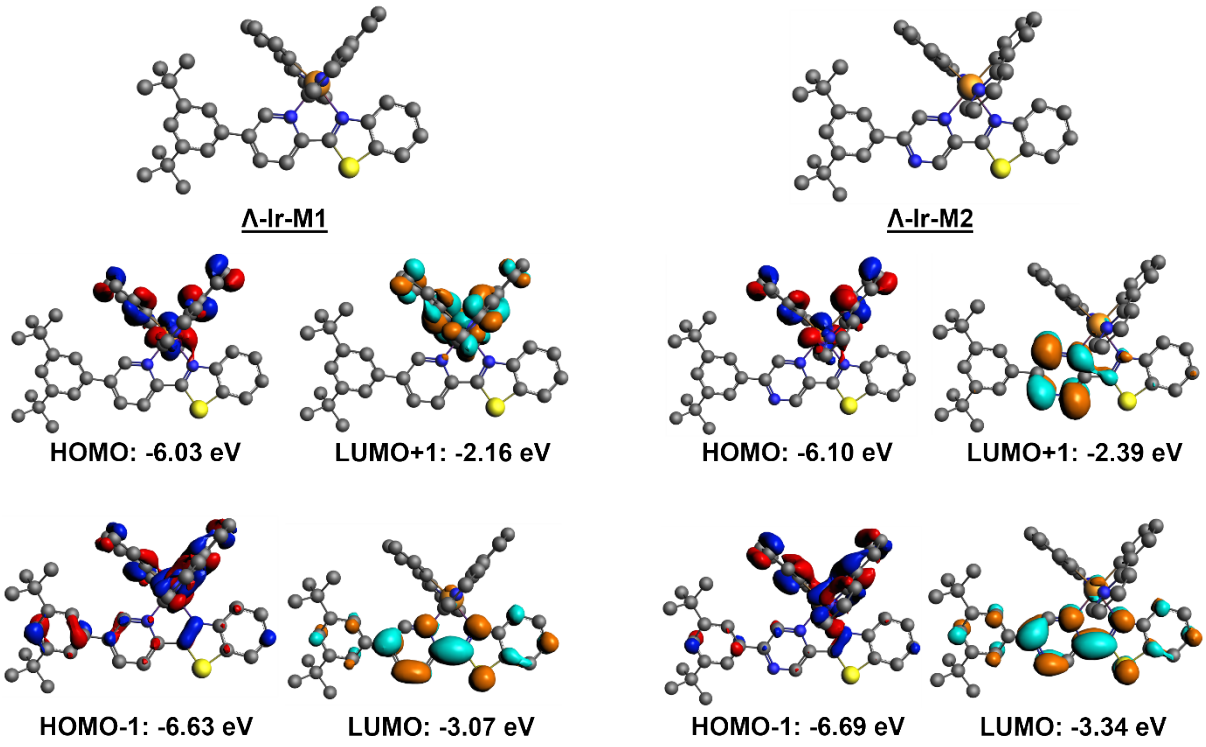

Figure S10. Frontier orbitals of ***Λ*-Ir-M1** and ***Λ*-Ir-M2**. Ir atoms are orange, S atoms are yellow, N atoms are blue and C atoms are grey. H atoms were eluded for visibility.

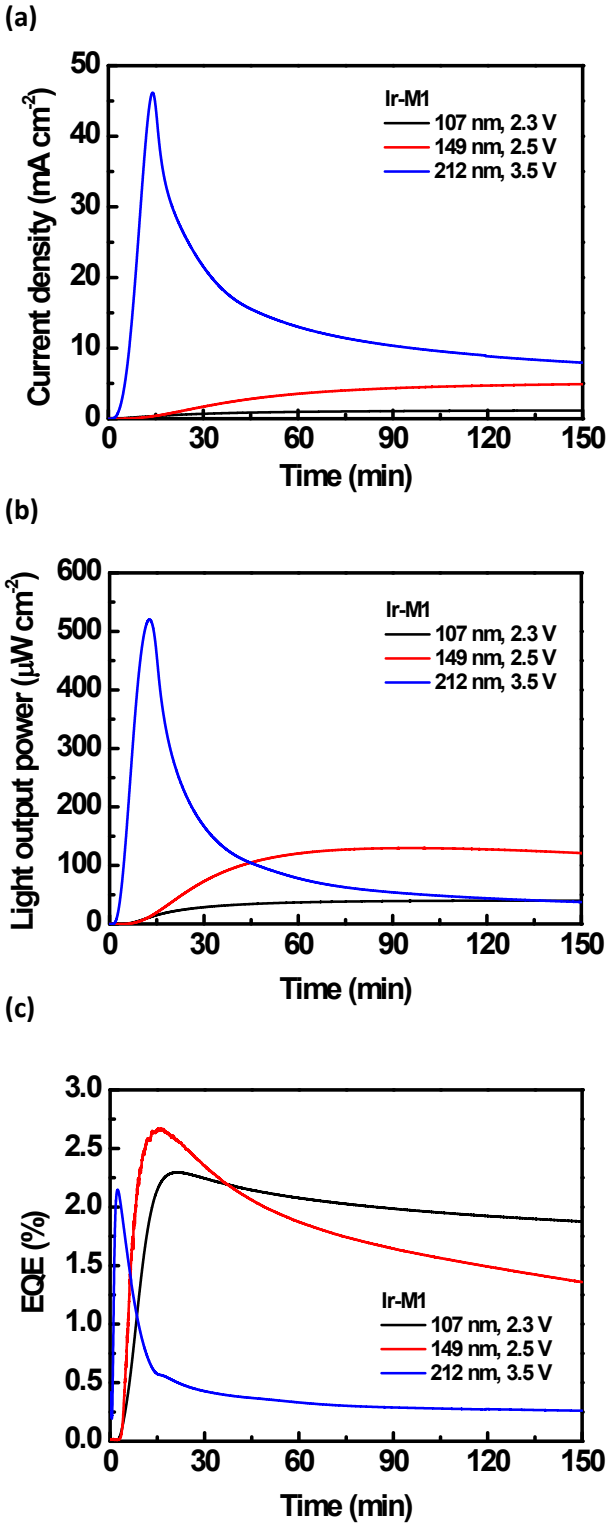

Figure S11. Time-dependent (a) current density, (b) light output, and (c) EQE of the LECs based on complex **Ir-M1**.

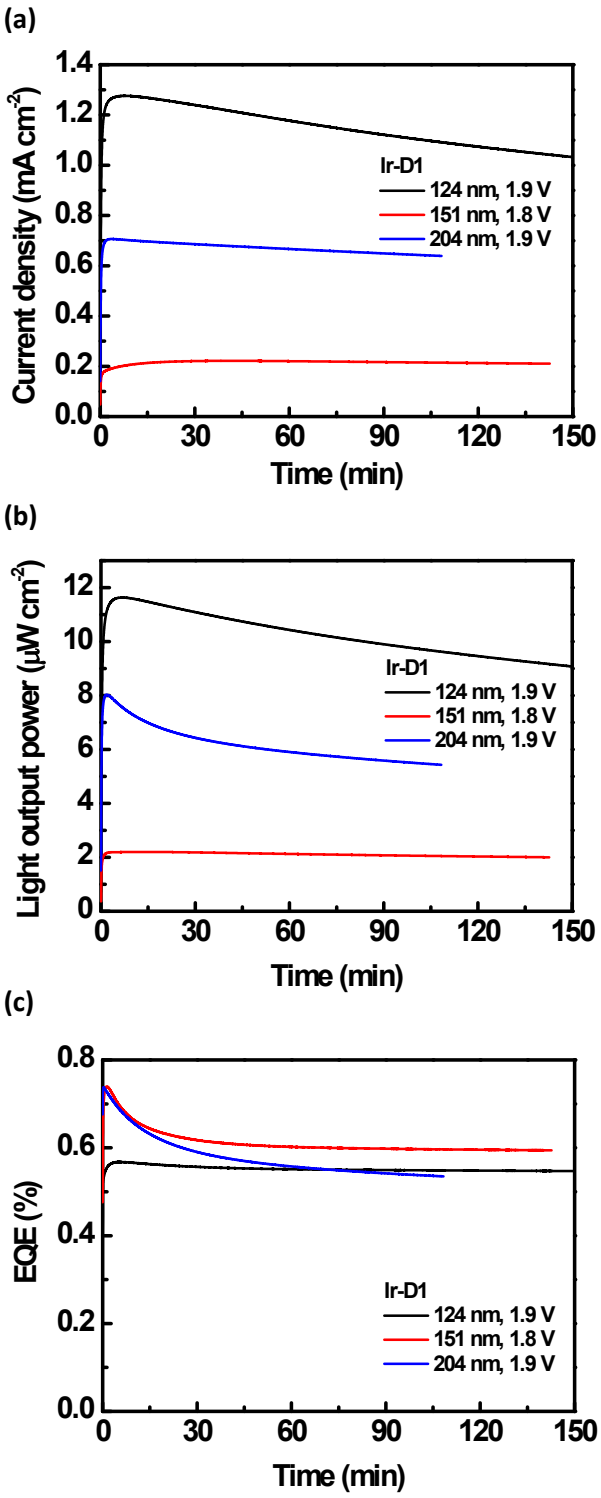

Figure S12. Time-dependent (a) current density, (b) light output, and (c) EQE of the LECs based on complex **Ir-D1**.

Chemical characterization

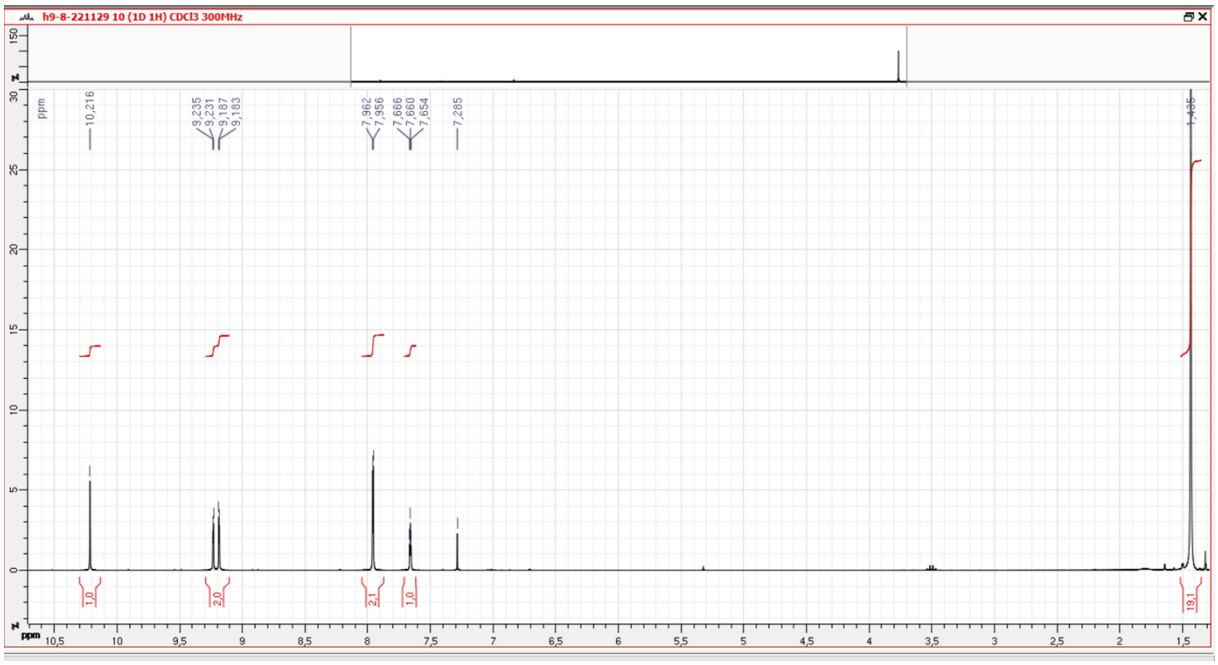

Figure S13. ^{1}H NMR (500 MHz, $CDCl_3$, 298 K) spectrum recorded for compound 5-(3,5-di-*tert*-butylphenyl)pyrazine-2-carbaldehyde.

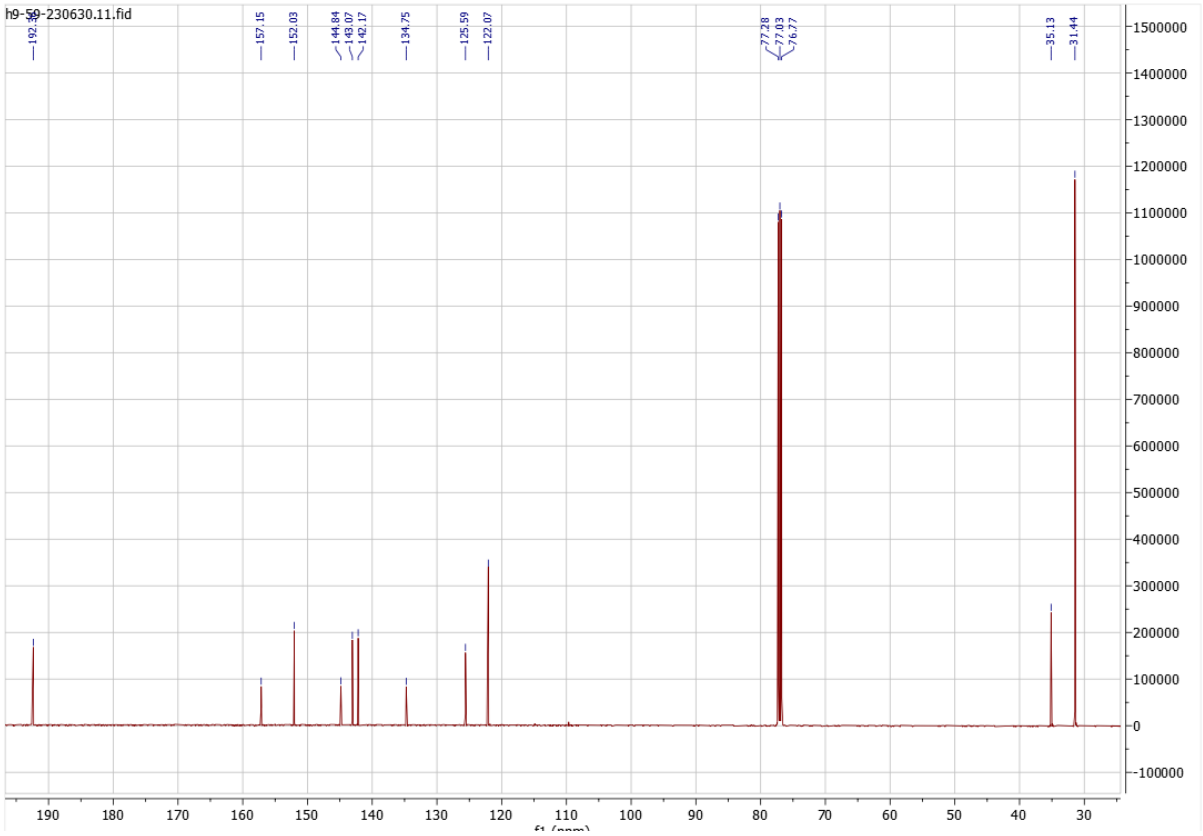

Figure S14. $^{13}C\{^{1}H\}$ NMR (125 MHz, $CDCl_3$, 298 K) spectrum recorded for compound 5-(3,5-di-*tert*-butylphenyl)pyrazine-2-carbaldehyde.

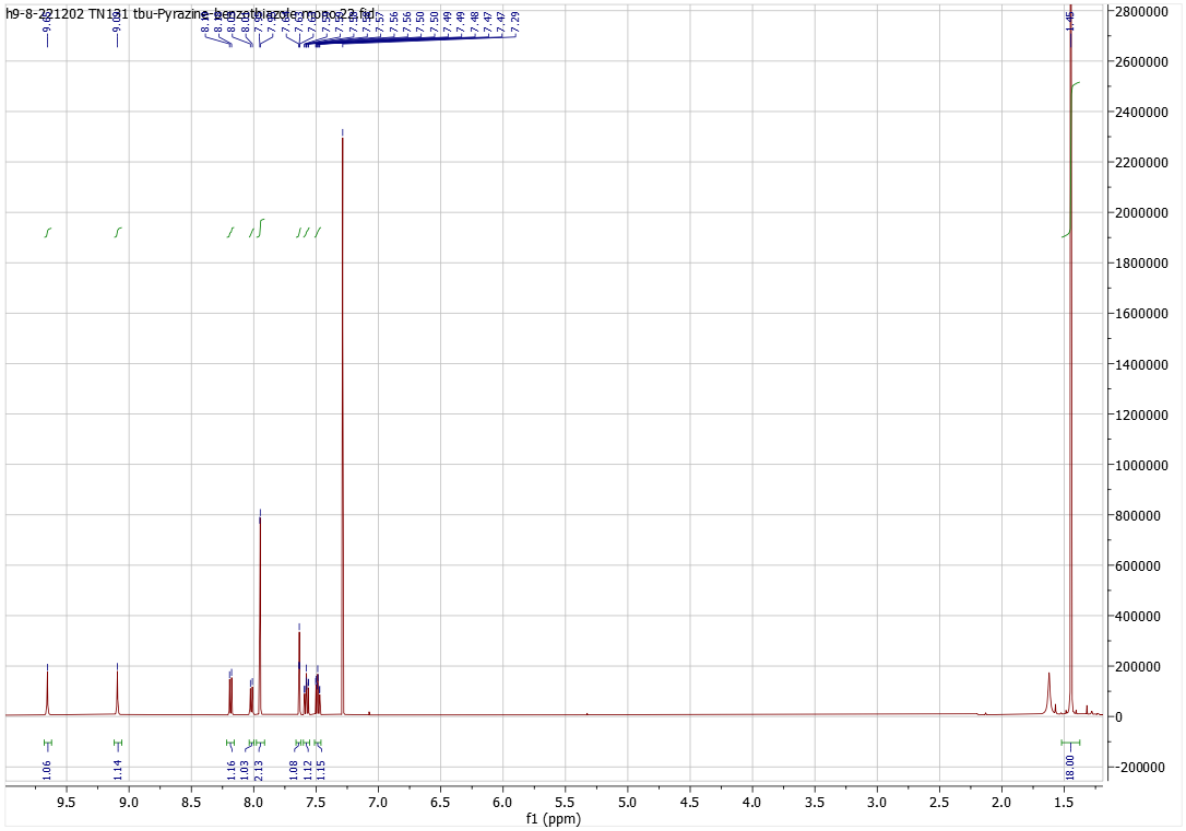

Figure S15. ^{1}H NMR (500 MHz, $CDCl_3$, 298 K) spectrum recorded for ligand **L2**.

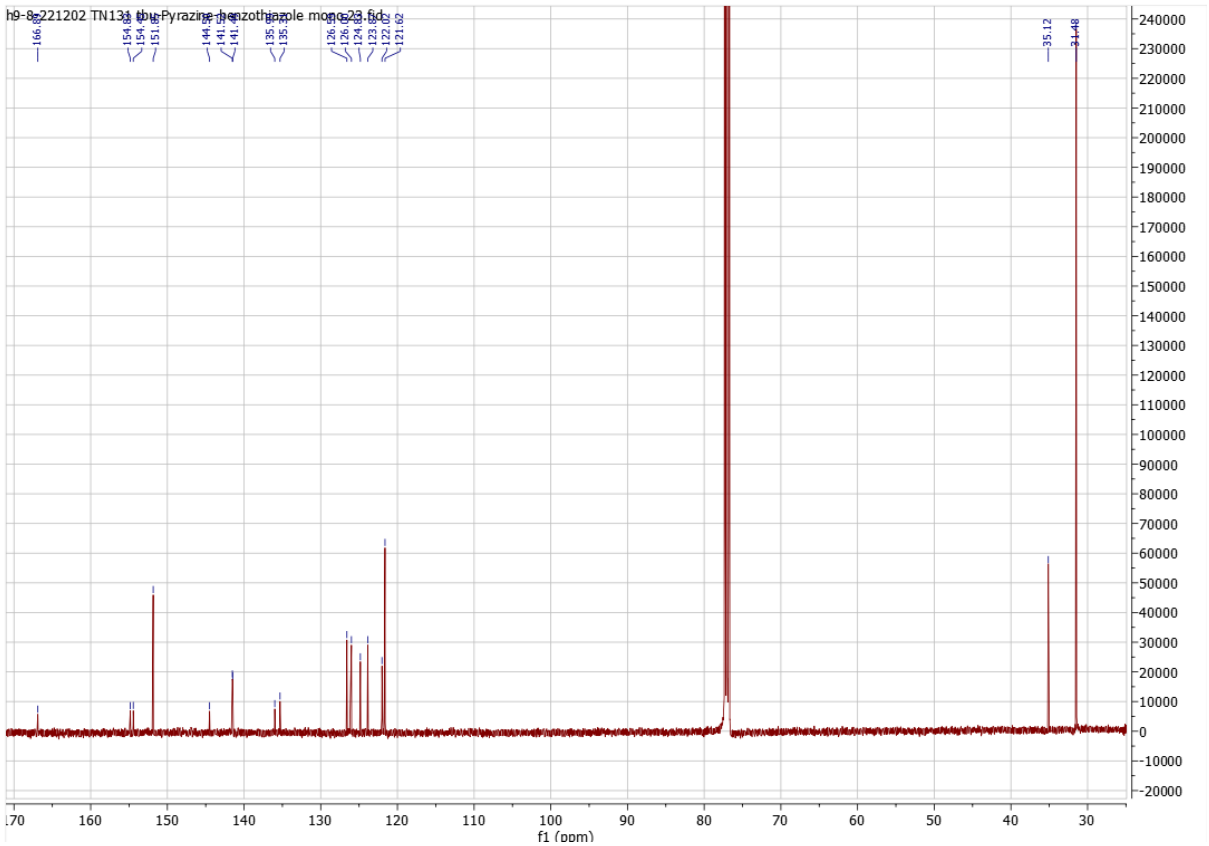

Figure S16. $^{13}C\{^{1}H\}$ NMR (125 MHz, $CDCl_3$, 298 K) spectrum recorded for ligand **L2**.

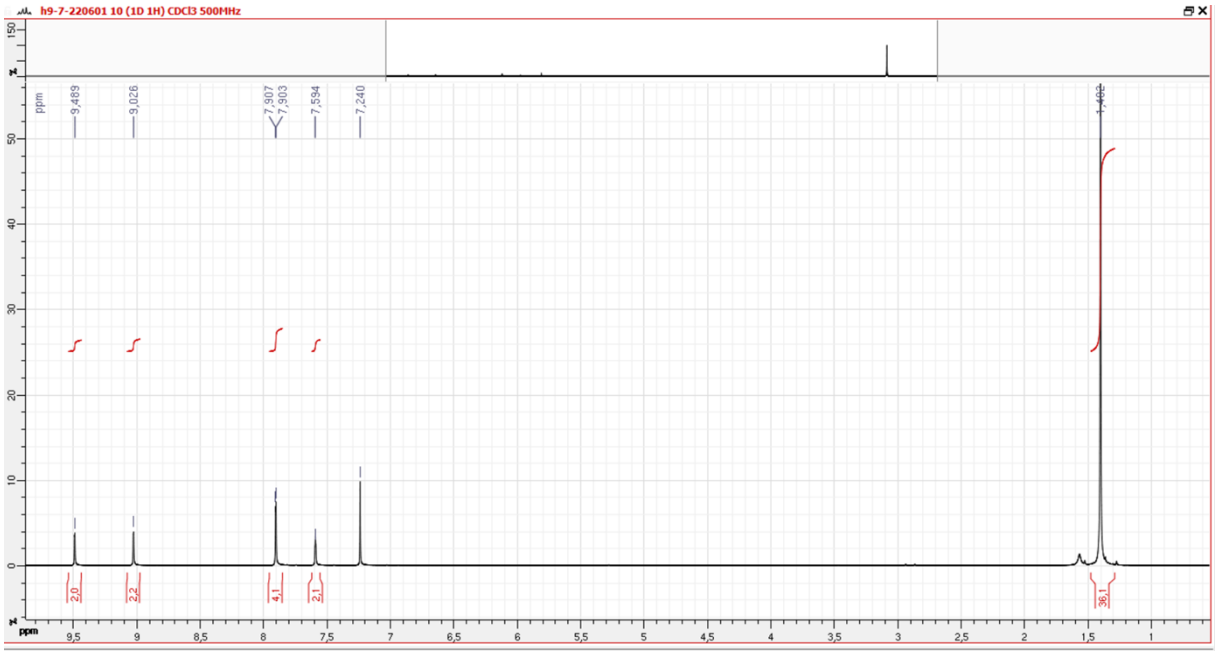

Figure S17. ^{1}H NMR (500 MHz, $CDCl_3$, 298 K) spectrum recorded for ligand **L4**.

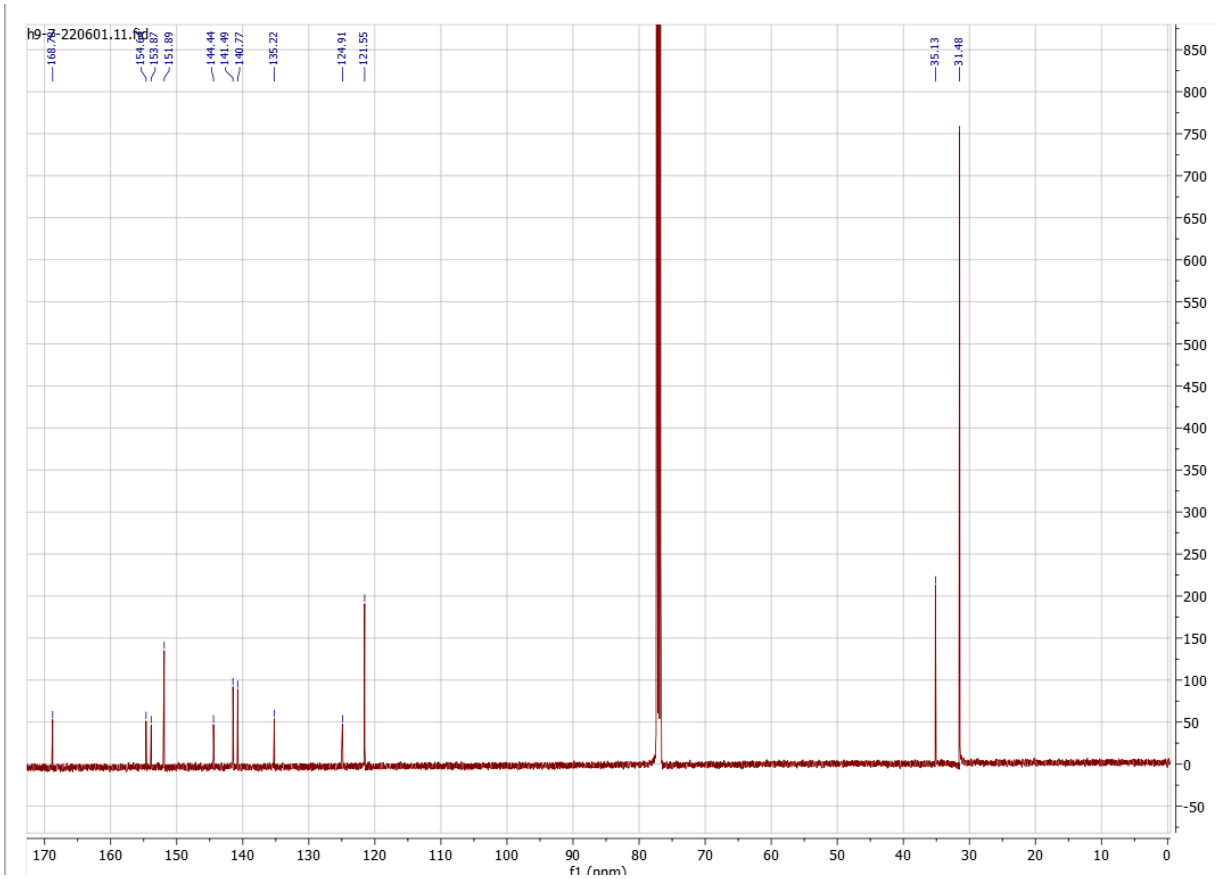

Figure S18. $^{13}C\{^{1}H\}$ NMR (125 MHz, $CDCl_3$, 298 K) spectrum recorded for ligand **L4**.

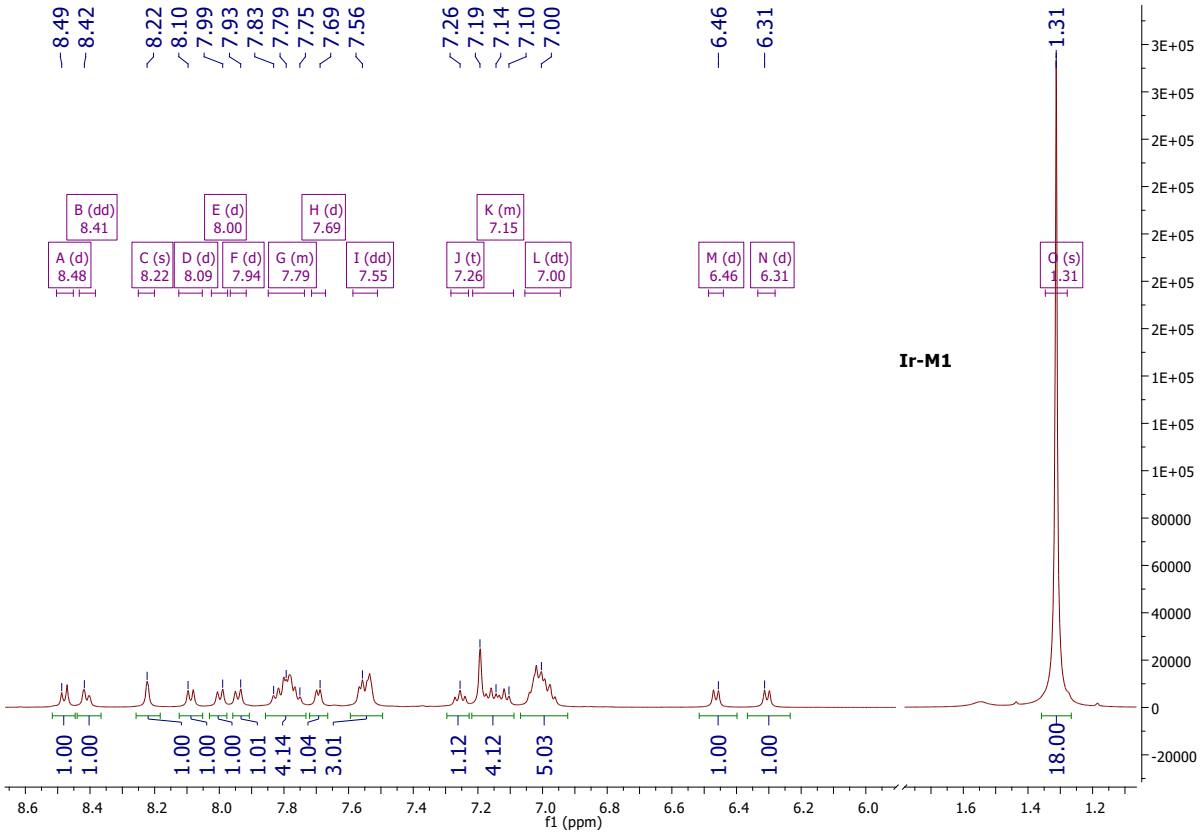

Figure S19. ^{1}H NMR (500 MHz, CD_2Cl_2, 298 K) spectrum recorded for complex **Ir-M1.**

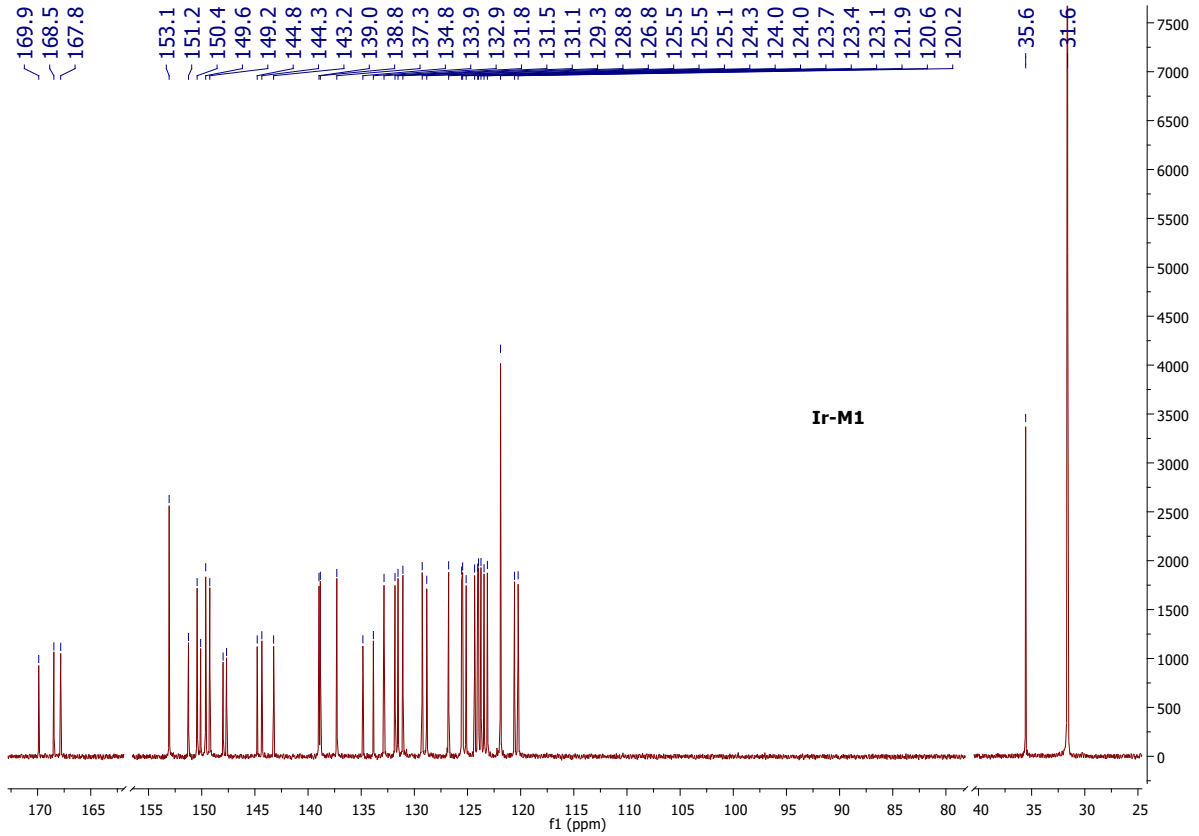

Figure S20. $^{13}C\{^{1}H\}$ NMR (126 MHz, CD_2Cl_2, 298 K) spectrum recorded for complex **Ir-M1**.

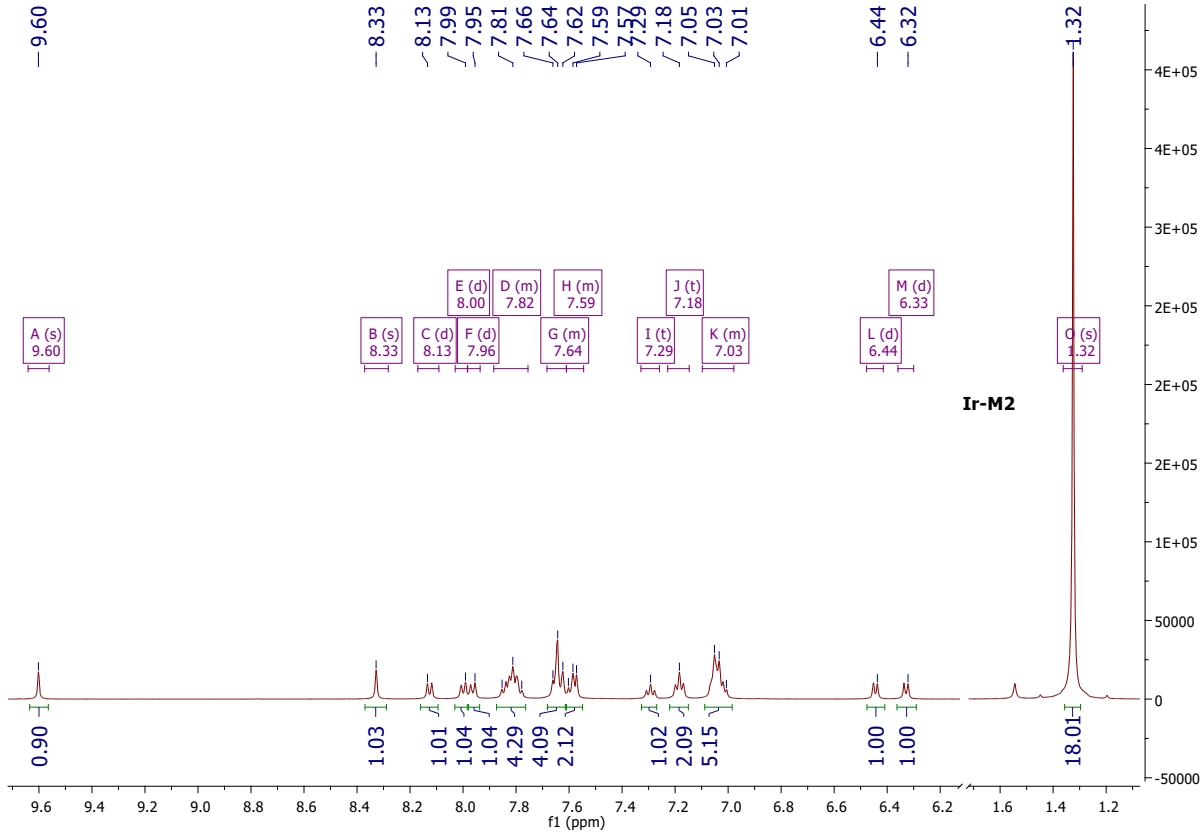

Figure S21. ^{1}H NMR (500 MHz, CD_2Cl_2, 298 K) spectrum recorded for complex **Ir-M2.**

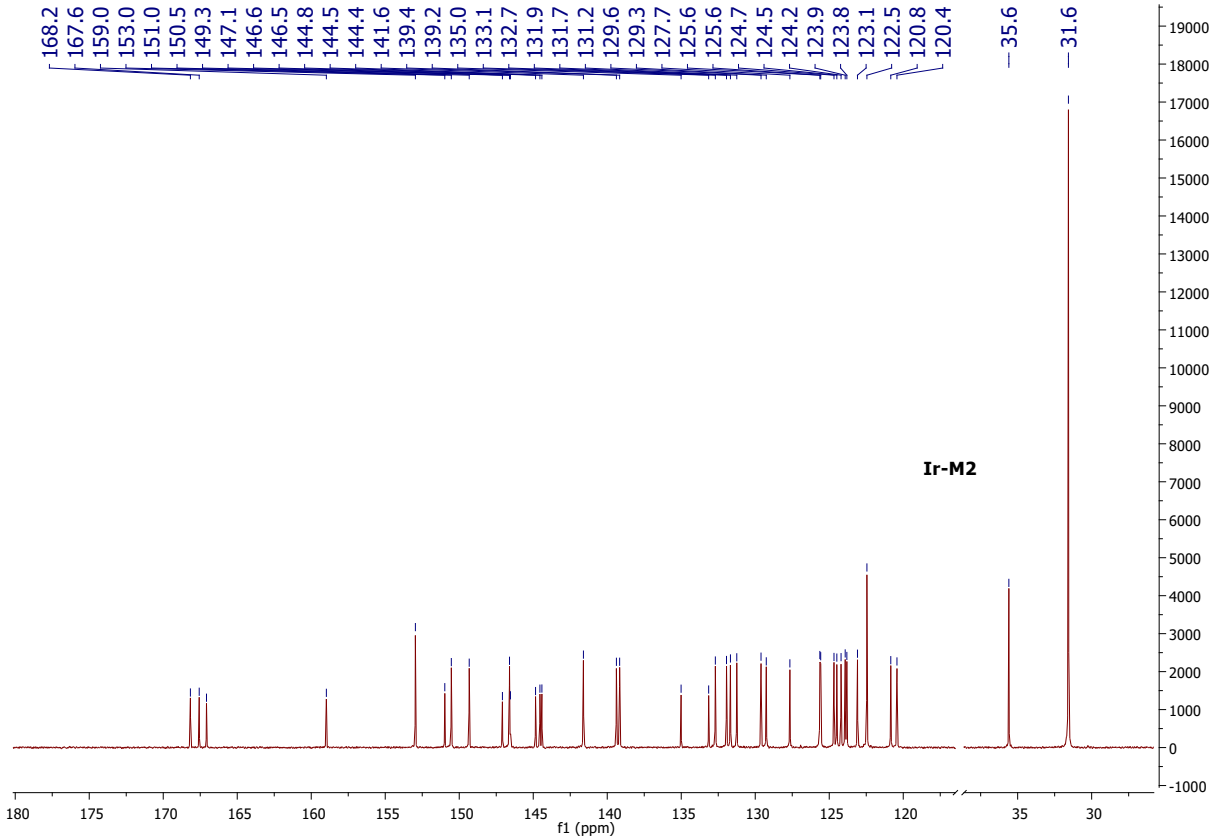

Figure S22. $^{13}C\{^{1}H\}$ NMR (126 MHz, CD_2Cl_2, 298 K) spectrum recorded for complex **Ir-M2**.

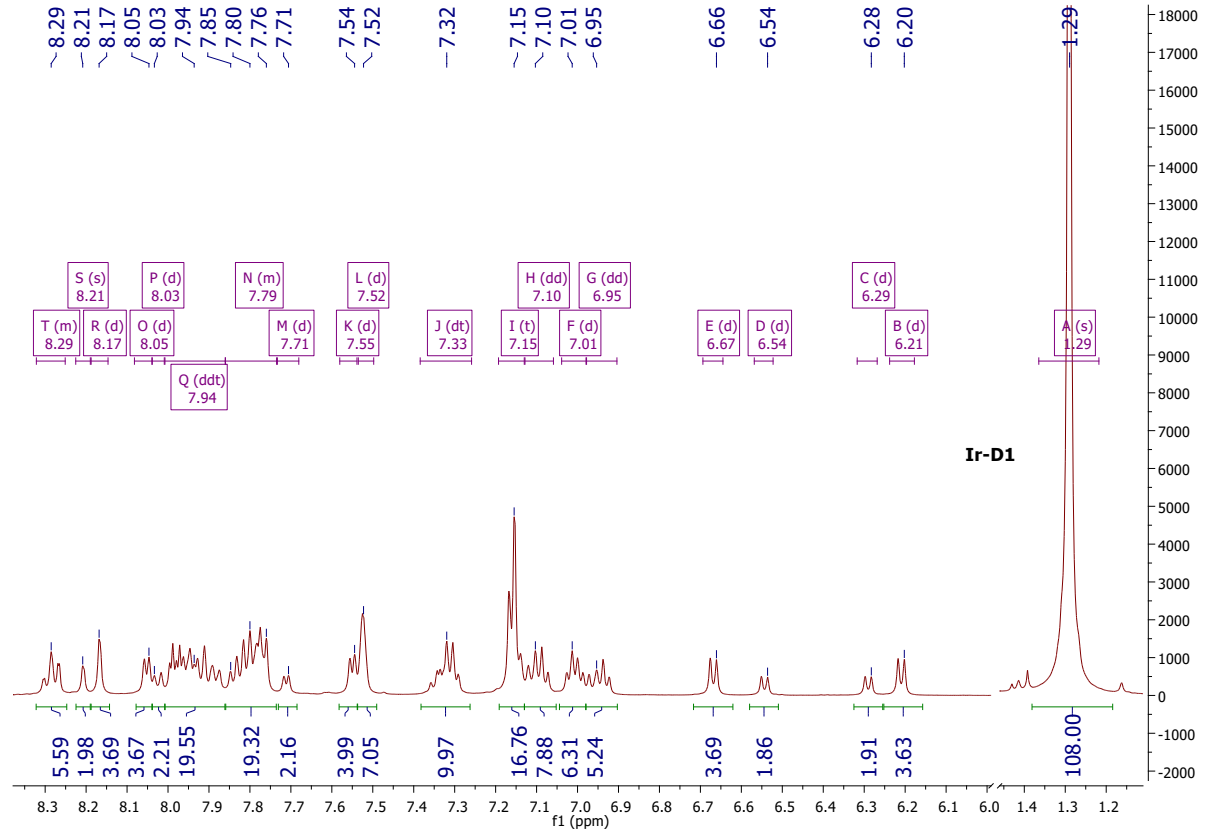

Figure S23. ^{1}H NMR (500 MHz, CD_2Cl_2, 298 K) spectrum recorded for complex **Ir-D1**.

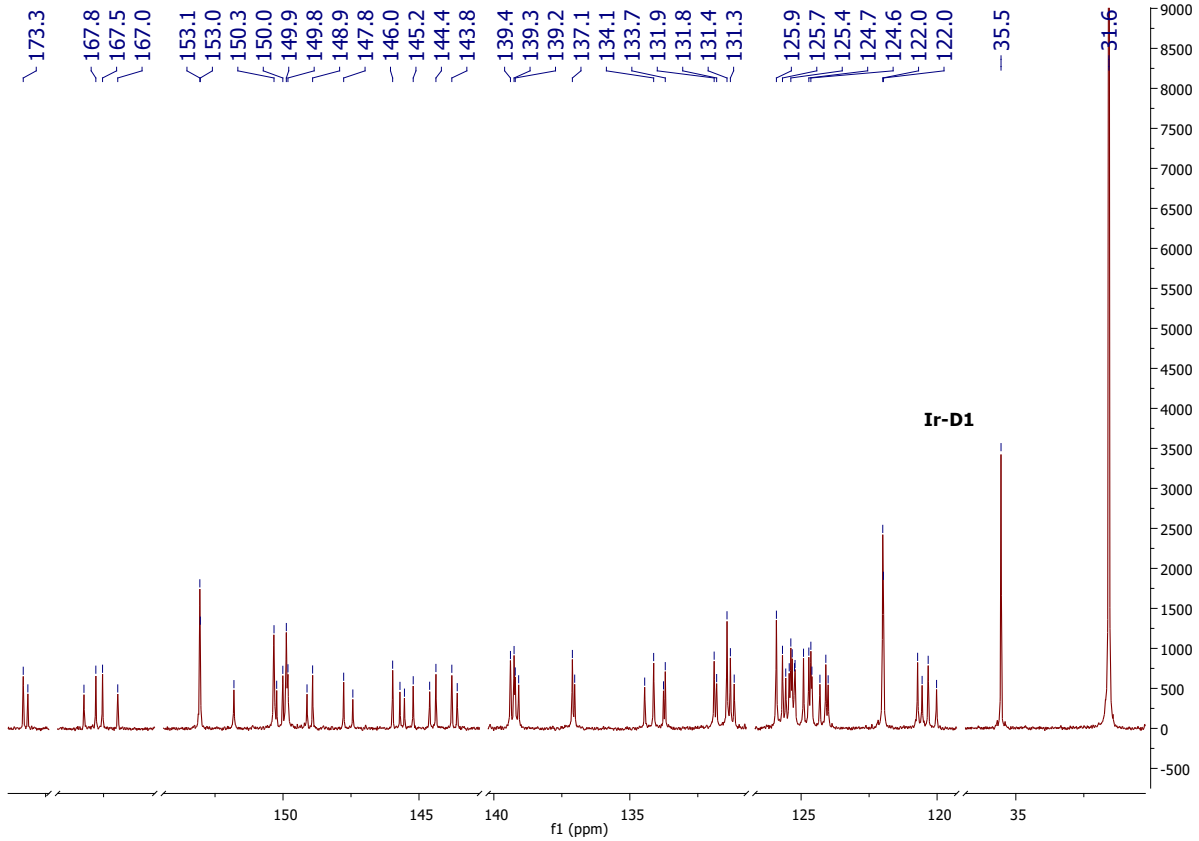

Figure S24. $^{13}C\{^{1}H\}$ NMR (126 MHz, CD_2Cl_2, 298 K) spectrum recorded for complex **Ir-D1.**

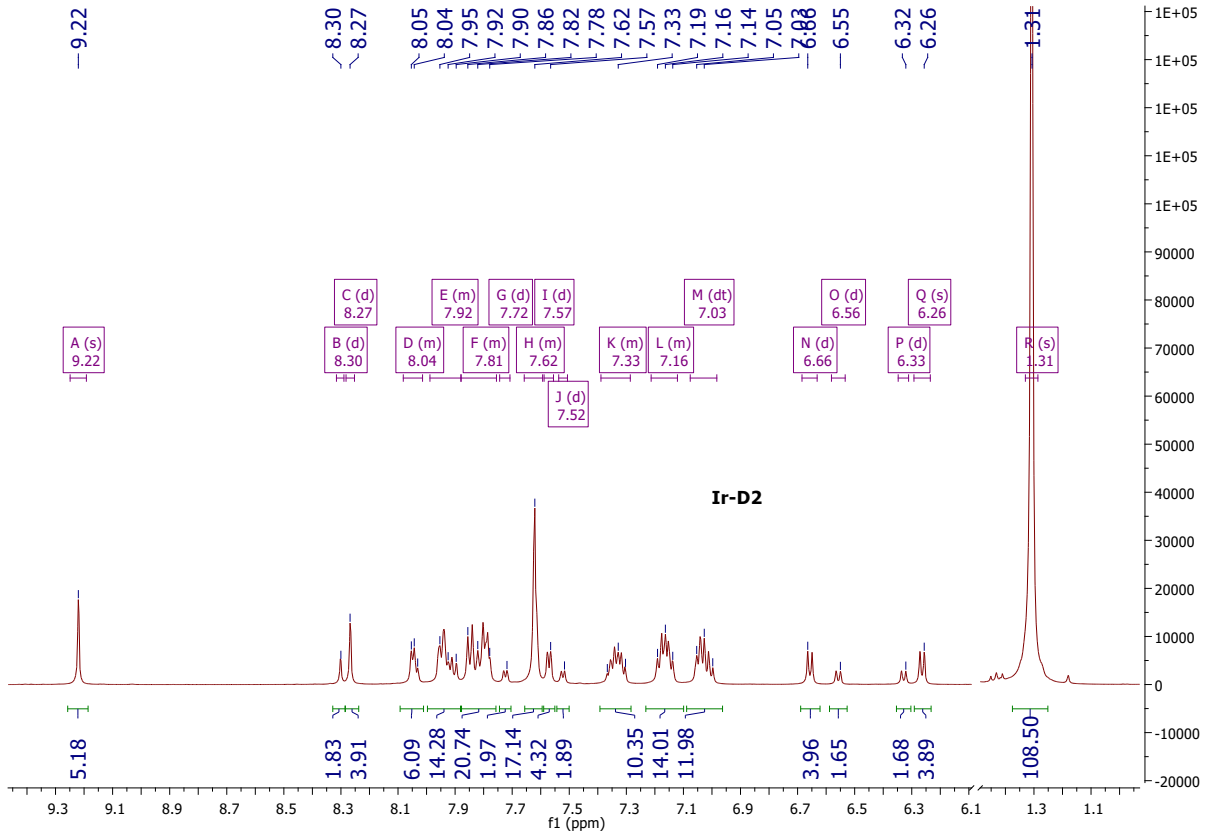

Figure S25. ^{1}H NMR (500 MHz, CD_2Cl_2, 298 K) spectrum recorded for complex **Ir-D2**.

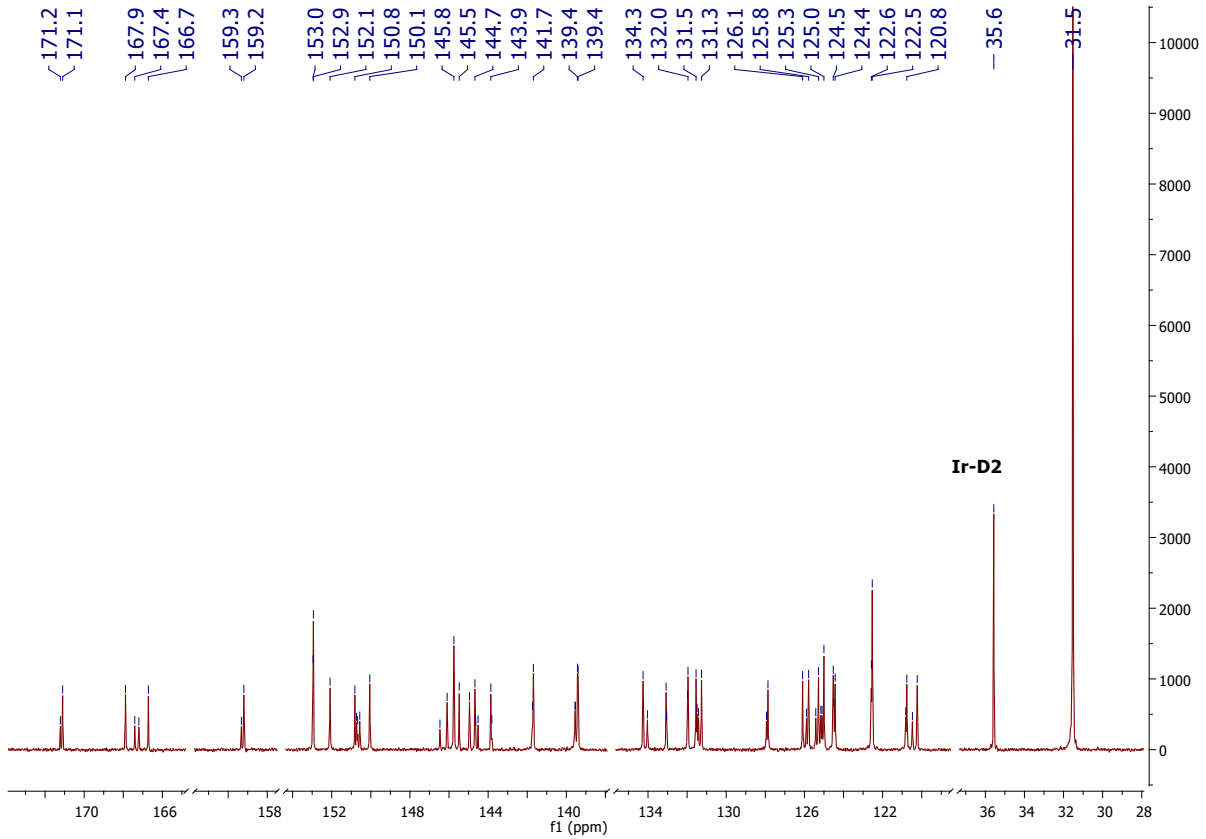

Figure S26. $^{13}C\{^{1}H\}$ NMR (126 MHz, CD_2Cl_2, 298 K) spectrum recorded for complex **Ir-D2**.

Mass spectra

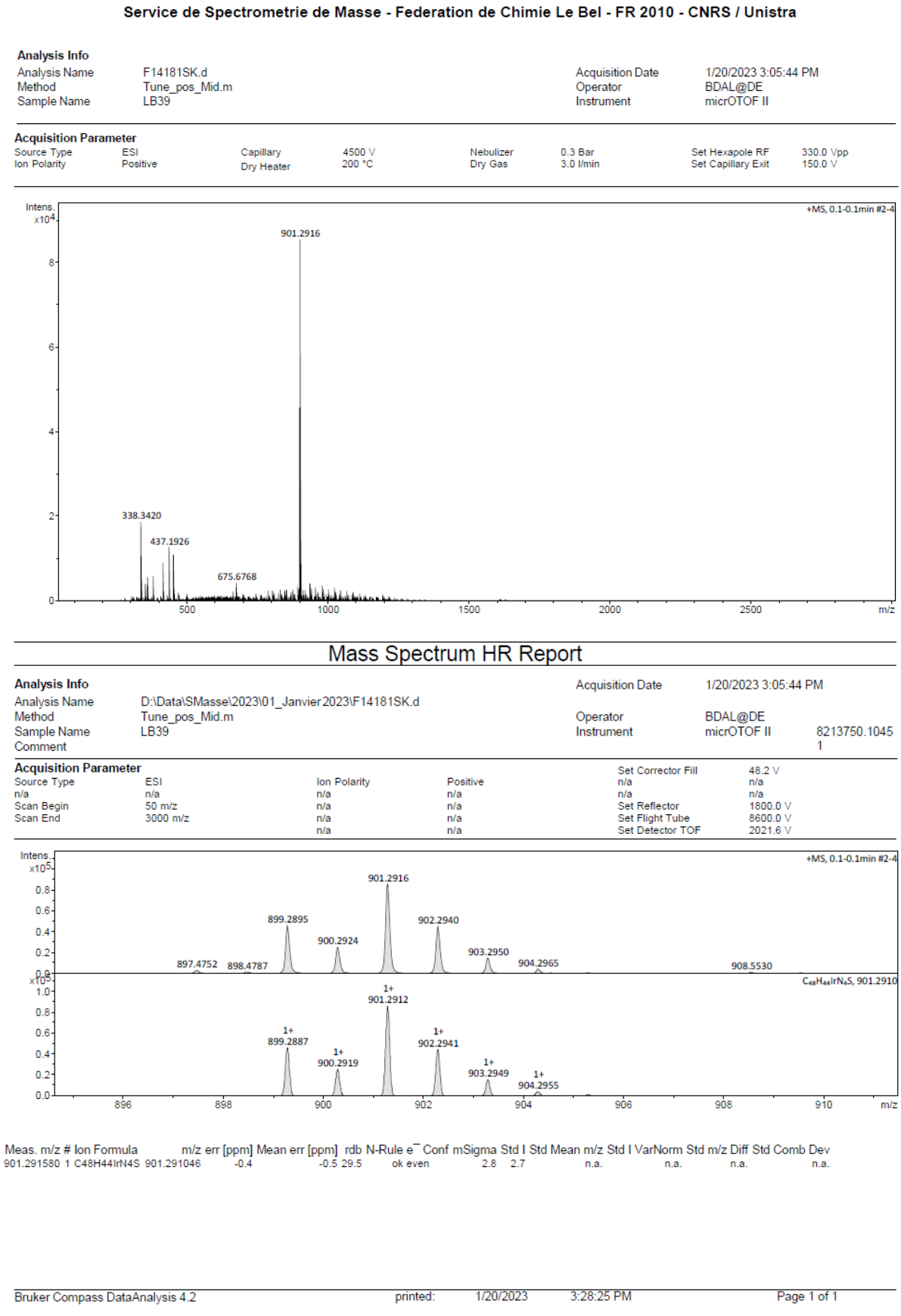

Figure S27. High-resolution HR-ESI-MS spectrum of compound **Ir-M1**.

Service de Spectrometrie de Masse - Federation de Chimie Le Bel - FR 2010 - CNRS / Unistra

Analysis Info

Analysis Name	F14179SK.d	Acquisition Date	1/20/2023 2:56:26 PM
Method	Tune_pos_Mid.m	Operator	BDAL@DE
Sample Name	LB40	Instrument	micrOTOF II

Acquisition Parameter

Source Type	ESI	Capillary	4500 V	Nebulizer	0.3 Bar	Set Hexapole RF	330.0 Vpp
Ion Polarity	Positive	Dry Heater	200 °C	Dry Gas	3.0 l/min	Set Capillary Exit	150.0 V

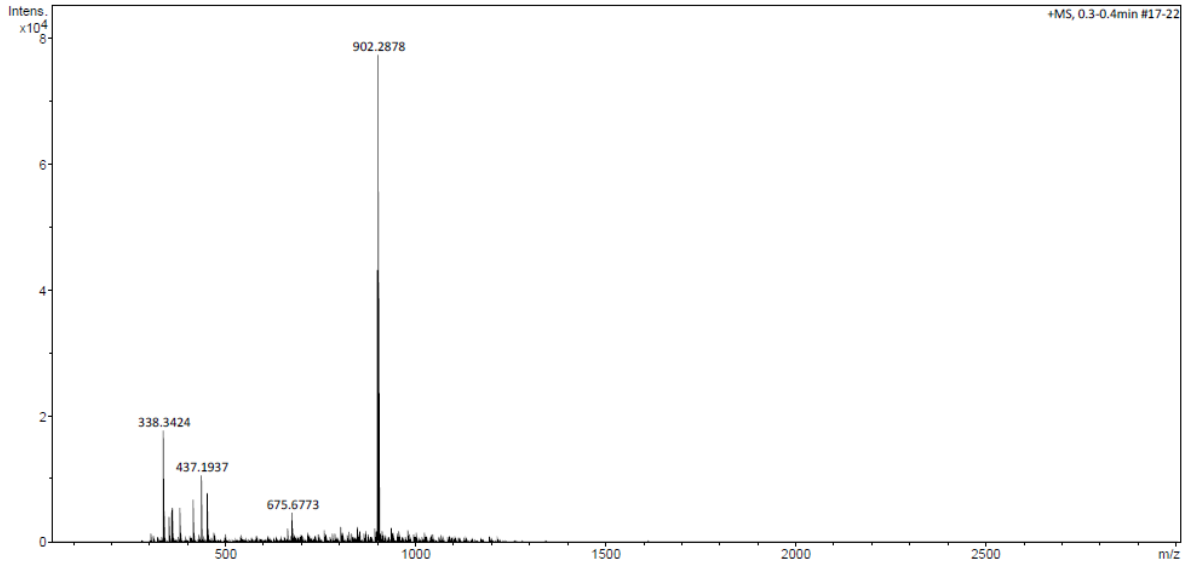

Mass Spectrum HR Report

Analysis Info

Analysis Name	D:\Data\SMasse\2023\01_Janvier 2023\F14179SK.d		
Method	Tune_pos_Mid.m	Acquisition Date	1/20/2023 2:56:26 PM
Sample Name	LB40	Operator	BDAL@DE
Comment		Instrument	micrOTOF II 8213750.1045 1

Acquisition Parameter

Source Type	ESI	Ion Polarity	Positive	Set Corrector Fill	48.2 V
n/a	n/a	n/a	n/a	n/a	n/a
Scan Begin	50 m/z	n/a	n/a	Set Reflector	1800.0 V
Scan End	3000 m/z	n/a	n/a	Set Flight Tube	8600.0 V
		n/a	n/a	Set Detector TOF	2021.6 V

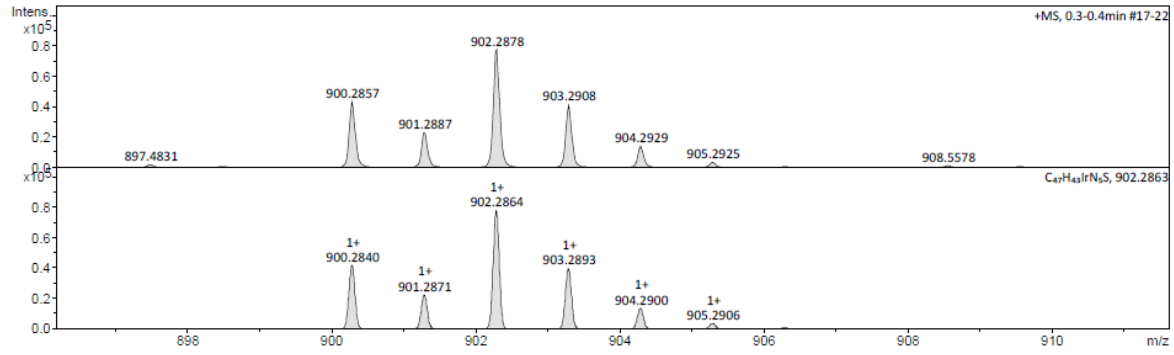

Meas. m/z	#	Ion Formula	m/z err [ppm]	Mean err [ppm]	rdb	N-Rule	e⁻ Conf	mSigma	Std I	Std Mean m/z	Std I	VarNorm Std m/z	Diff Std Comb	Dev
902.287819	1	C47H43IrN5S	902.286295	-1.5	-1.9	29.5	ok	even	13.4	10.4	n.a.	n.a.	n.a.	n.a.

Bruker Compass DataAnalysis 4.2 printed: 1/20/2023 3:32:27 PM Page 1 of 1

Figure S28. High-resolution HR-ESI-MS spectrum of compound **Ir-M2**.

Service de Spectrométrie de Masse - Fédération de Chimie Le Bel - FR 2010 - CNRS / UDS

Analysis Info

Analysis Name	O46157SK.d	Acquisition Date	15/11/2022 16:53:49
Method	esi wide pos.m	Operator	admin
Sample Name	LB35	Instrument	micrOTOF
Comment			

Acquisition Parameter

Source Type	ESI	Capillary	4500 V	Nebulizer	0.5 Bar	Corona	195 nA
Ion Polarity	Positive	Set Capillary Exit	150.0 V	Dry Gas	4.0 l/min	Set Hexapole RF	300.0 V
n/a	n/a	Set Skimmer 1	50.0 V	Dry Heater	200 °C	APCI Heater	514 °C

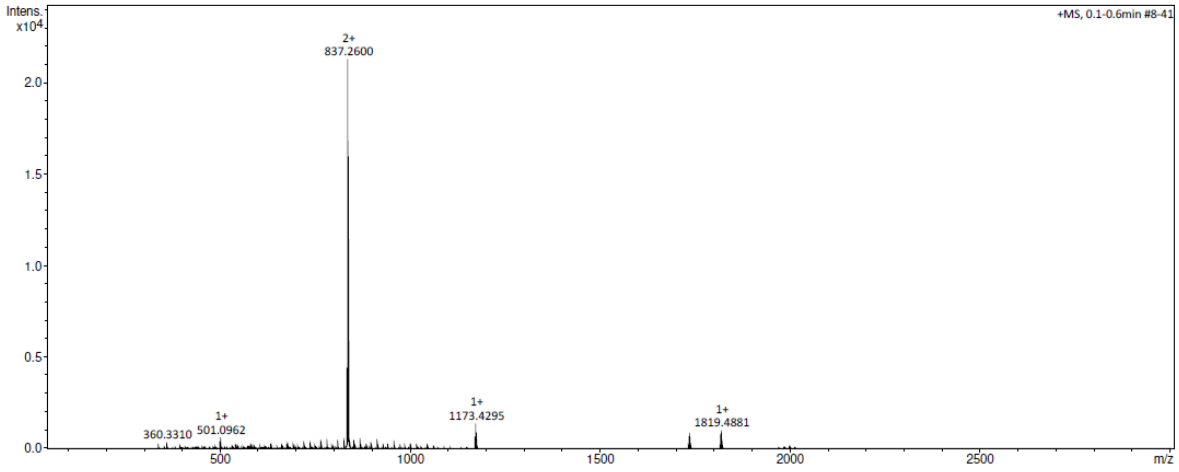

Bruker Daltonics DataAnalysis 3.1 printed: 16/11/2022 10:47:39 Page 1 of 1

Mass Spectrum HR Report

Analysis Info

Analysis Name	Z:\O46157SK.d	Acquisition Date	15/11/2022 16:53:49	
Method	esi wide pos.m			
Sample Name	LB35	Operator	admin	
Comment		Instrument	micrOTOF	213750.00066

Acquisition Parameter

Source Type	ESI	Ion Polarity	Positive	Set Corrector Fill	74 V
n/a	n/a	Set Capillary Exit	150.0 V	Set Pulsar Pull	799 V
Scan Begin	50 m/z	Set Hexapole RF	300.0 V	Set Pulsar Push	799 V
Scan End	3000 m/z	Set Skimmer 1	50.0 V	Set Reflector	1700 V
		Set Hexapole 1	24.3 V	Set Flight Tube	8600 V
				Set Detector TOF	2311 V

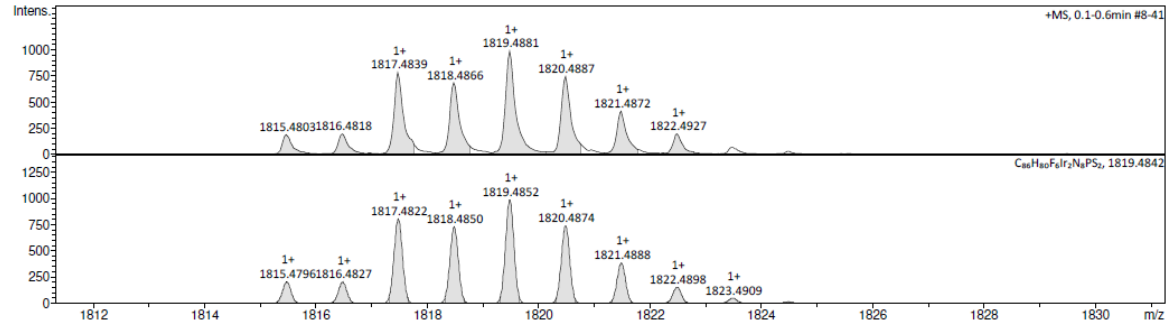

Meas. m/z	#	Ion Formula	m/z	err [ppm]	mSigma	# mSigma	Score	rdb	e⁻ Conf	N-Rule
837.2600	1	C86H80Ir2N8S2	837.2597	0.3	10.7	1	100.00	52.0	even	ok
1819.4881	1	C86H80F6Ir2N8PS2	1819.4842	-1.6	29.1	1	100.00	49.5	even	ok

Bruker Compass DataAnalysis 4.2 printed: 16/11/2022 10:46:29 Page 1 of 1

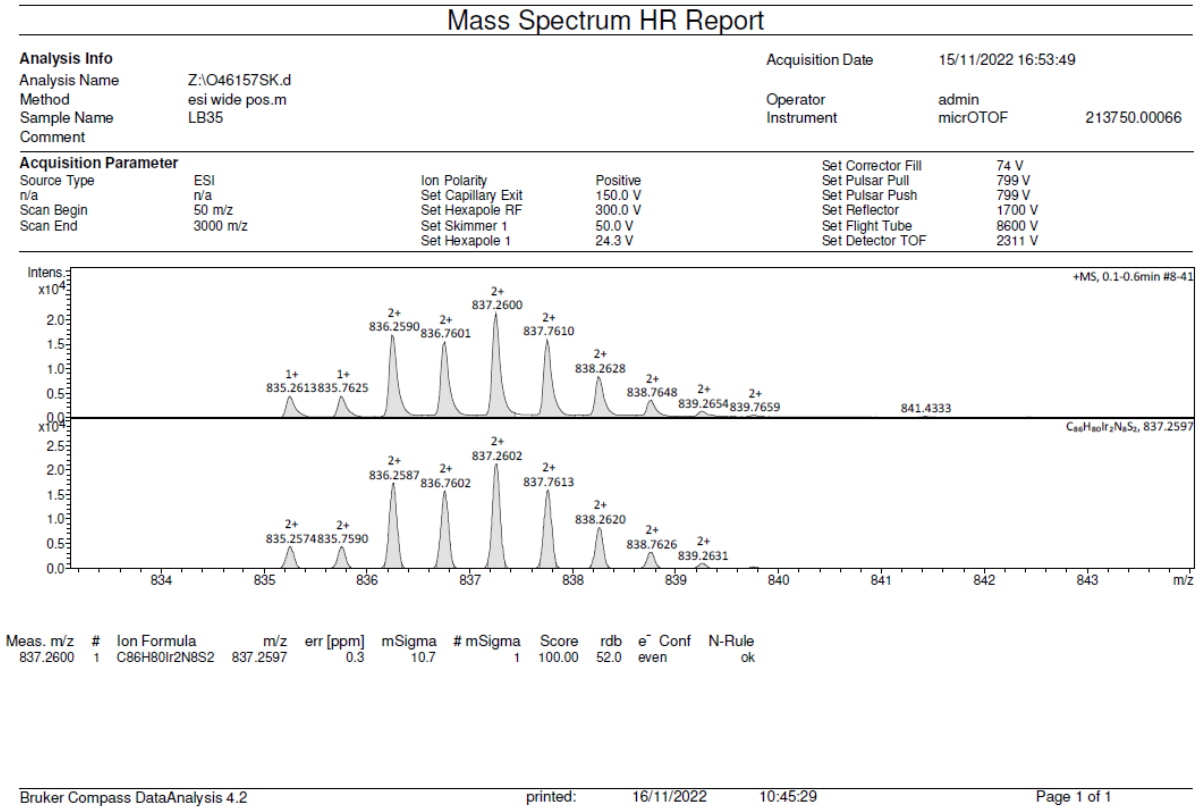

Meas. m/z	#	Ion Formula	m/z	err [ppm]	mSigma	# mSigma	Score	rdb	e⁻ Conf	N-Rule
837.2600	1	C86H80Ir2N8S2	837.2597	0.3	10.7	1	100.00	52.0	even	ok

Bruker Compass DataAnalysis 4.2 printed: 16/11/2022 10:45:29 Page 1 of 1

Figure S29. High-resolution HR-ESI-MS spectrum of compound **Ir-D1**.

Service de Spectrométrie de Masse - Fédération de Chimie Le Bel - FR 2010 - CNRS / UDS

Analysis Info

Analysis Name	O46159SK.d	Acquisition Date	15/11/2022 17:04:09
Method	esi wide pos.m	Operator	admin
Sample Name	LB34	Instrument	micrOTOF
Comment			

Acquisition Parameter

Source Type	ESI	Capillary	4500 V	Nebulizer	0.5 Bar	Corona	195 nA
Ion Polarity	Positive	Set Capillary Exit	150.0 V	Dry Gas	4.0 l/min	Set Hexapole RF	300.0 V
n/a	n/a	Set Skimmer 1	50.0 V	Dry Heater	200 °C	APCI Heater	514 °C

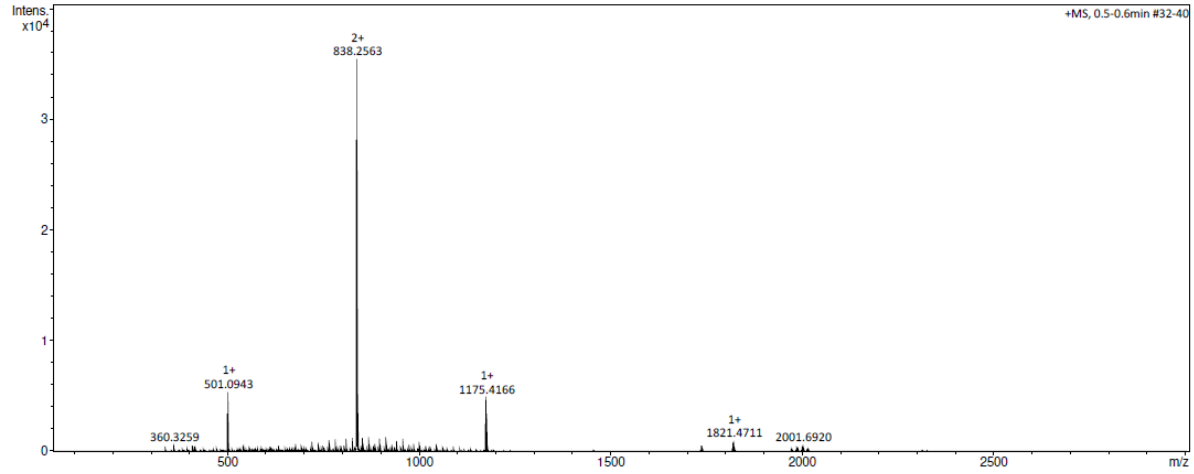

Bruker Daltonics DataAnalysis 3.1 printed: 16/11/2022 11:02:41 Page 1 of 1

Mass Spectrum HR Report

Analysis Info

Analysis Name	Z:\O46159SK.d	Acquisition Date	15/11/2022 17:04:09
Method	esi wide pos.m	Operator	admin
Sample Name	LB34	Instrument	micrOTOF 213750.00066
Comment			

Acquisition Parameter

Source Type	ESI	Ion Polarity	Positive	Set Corrector Fill	74 V
n/a	n/a	Set Capillary Exit	150.0 V	Set Pulsar Pull	799 V
Scan Begin	50 m/z	Set Hexapole RF	300.0 V	Set Pulsar Push	799 V
Scan End	3000 m/z	Set Skimmer 1	50.0 V	Set Reflector	1700 V
		Set Hexapole 1	24.3 V	Set Flight Tube	8600 V
				Set Detector TOF	2311 V

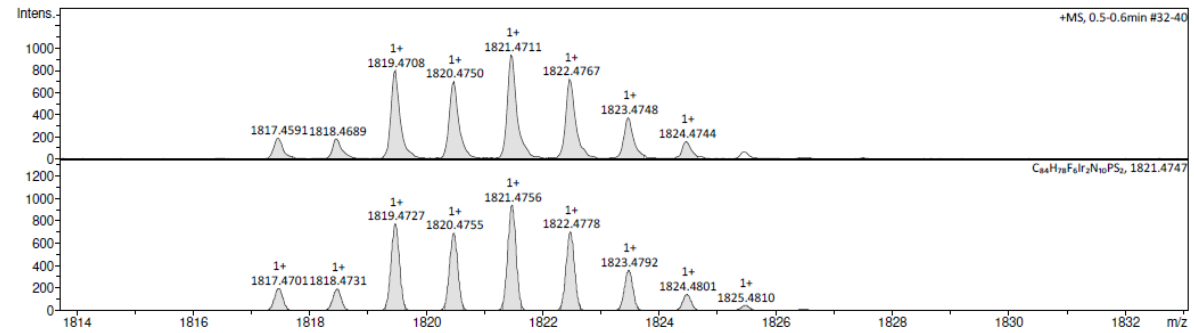

Meas. m/z	#	Ion Formula	m/z	err [ppm]	mSigma	# mSigma	Score	rdb	e⁻ Conf	N-Rule
838.2563	1	C84H78Ir2N10S2	838.2550	-1.0	12.1	1	100.00	52.0	even	ok
1821.4711	1	C84H78F6Ir2N10PS2	1821.4747	2.4	23.1	1	100.00	49.5	even	ok

Bruker Compass DataAnalysis 4.2 printed: 16/11/2022 11:02:10 Page 1 of 1

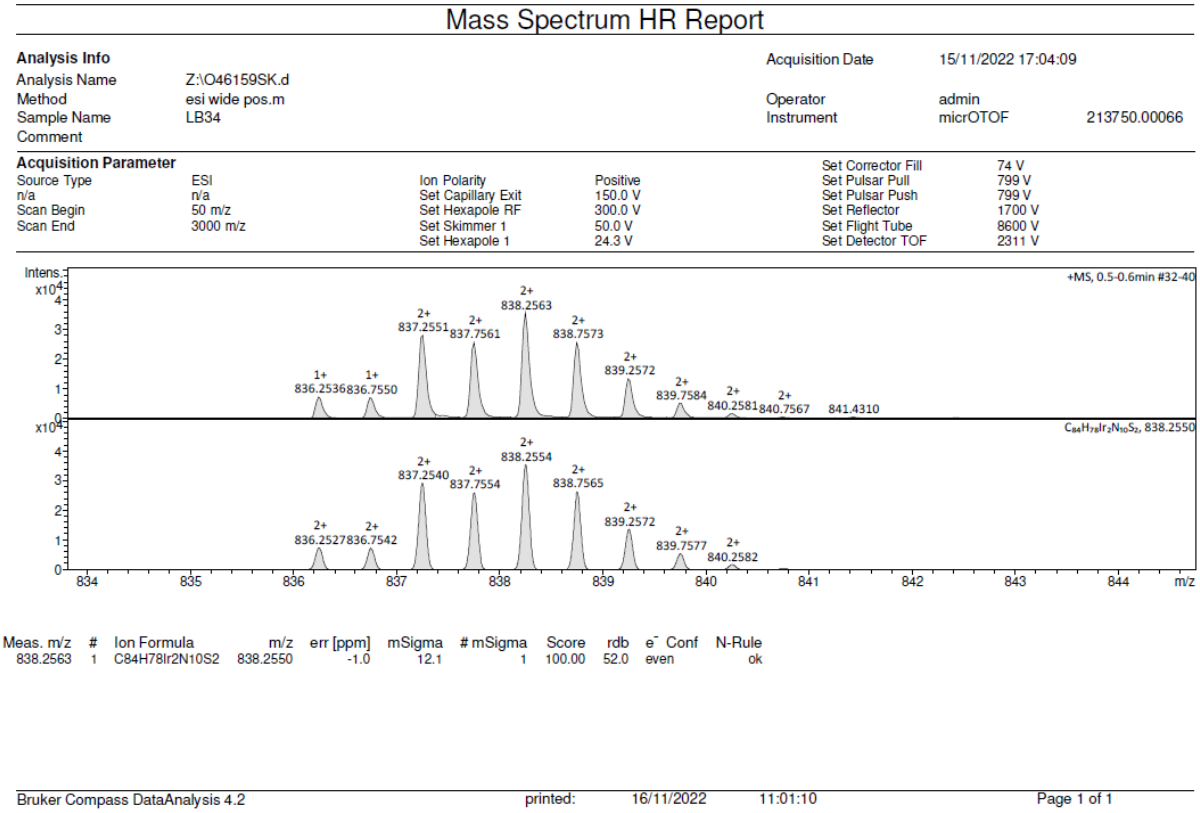

Figure S30. High-resolution HR-ESI-MS spectrum of compound **Ir-D2**.

Supplementary Tables

Table S1. Crystal data and structure refinement for compound **Ir-M1 (CCDC 2338499)**.

Identification code	emmlb230306sq	
Empirical formula	C48 H44 F6 Ir N4 P S, solvent 'C48 H44 Ir N4 S, F6 P,solvent'	
Formula weight	1046.10	
Temperature	173(2) K	
Wavelength	0.71073 Å	
Crystal system, space group	Monoclinic, P 21/c	
Unit cell dimensions	*a* = 9.1429(7) Å	α = 90°
	b = 19.1054(14) Å	β = 95.933(3)°
	c = 26.870(2) Å	γ = 90°
Volume	4668.5(6) $Å^3$	
Z, Calculated density	4, 1.488 Mg/m^3	
Absorption coefficient	3.000 mm^{-1}	
F(000)	2088	
Crystal size	0.180 x 0.100 x 0.100 mm	
Theta range for data collection	1.524 to 28.005°	
Limiting indices	-12<=h<=12, -25<=k<=25, -35<=l<=35	
Reflections collected / unique	261434 / 11241 [R(int) = 0.1648]	
Completeness to theta = 25.242	100.0%	
Absorption correction	Semi-empirical from equivalents	
Max. and min. transmission	0.7456 and 0.6547	
Refinement method	Full-matrix least-squares on F^2	
Data / restraints / parameters	11241 / 85 / 611	
Goodness-of-fit on F^2	1.005	
Final R indices [I>2sigma(I)]	R1 = 0.0427, wR2 = 0.0863	
R indices (all data)	R1 = 0.0790, wR2 = 0.0997	
Extinction coefficient	n/a	
Largest diff. peak and hole	2.687 and -0.738 *e* $Å^{-3}$	

Table S2. Crystal data and structure refinement for compound **Ir-M2 (CCDC 2338500)**.

Identification code	emmlb230206sq
Empirical formula	C47 H43 F6 Ir N5 P S, solvent 'C47 H43 Ir N5 S, F6 P, solvent'
Formula weight	1047.09
Temperature	173(2) K
Wavelength	0.71073 Å
Crystal system, space group	Triclinic, P -1
Unit cell dimensions	a = 13.393(4) Å α = 72.225(9)° b = 13.862(4) Å β = 81.792(10)° c = 13.953(4) Å γ = 70.801(11)°
Volume	2326.9(11) Å^3
Z, Calculated density	2, 1.494 Mg/m^3
Absorption coefficient	3.010 mm^{-1}
F(000)	1044
Crystal size	0.100 x 0.090 x 0.090 mm
Theta range for data collection	1.612 to 28.258°
Limiting indices	-17<=h<=16, -18<=k<=18, -18<=l<=18
Reflections collected / unique	52750 / 11335 [R(int) = 0.1102]
Completeness to theta = 25.242	100.0%
Absorption correction	Semi-empirical from equivalents
Max. and min. transmission	0.7456 and 0.6819
Refinement method	Full-matrix least-squares on F^2
Data / restraints / parameters	11335 / 6 / 539
Goodness-of-fit on F^2	1.008
Final R indices [I>2sigma(I)]	R1 = 0.0573, wR2 = 0.0953
R indices (all data)	R1 = 0.1211, wR2 = 0.1142
Extinction coefficient	n/a
Largest diff. peak and hole	2.022 and -1.316 e Å^{-3}

Table S3. Crystal data and structure refinement for compound **Ir-D1 (CCDC 2338501)**.

Identification code	mmlb230609	
Empirical formula	C92 H92 Cl12 F12 Ir2 N8 P2 S2	
Formula weight	2473.59	
Temperature	120(2) K	
Wavelength	0.71073 Å	
Crystal system, space group	Triclinic, P -1	
Unit cell dimensions	a = 12.8187(5) Å	α = 109.656(2)°
	b = 14.2975(6) Å	β = 108.743(2)°
	c = 16.2225(8) Å	γ = 101.975(2)°
Volume	2479.90(19) $Å^3$	
Z, Calculated density	1, 1.656 Mg/m^3	
Absorption coefficient	3.150 mm^{-1}	
F(000)	1228	
Crystal size	0.100 x 0.080 x 0.060 mm	
Theta range for data collection	1.944 to 30.074°	
Limiting indices	-16<=h<=18, -20<=k<=20, -22<=l<=22	
Reflections collected / unique	81496 / 14497 [R(int) = 0.0632]	
Completeness to theta = 25.242	99.9%	
Absorption correction	Semi-empirical from equivalents	
Max. and min. transmission	0.7460 and 0.6895	
Refinement method	Full-matrix least-squares on F^2	
Data / restraints / parameters	14497 / 0 / 595	
Goodness-of-fit on F^2	1.031	
Final R indices [I>2sigma(I)]	R1 = 0.0357, wR2 = 0.0722	
R indices (all data)	R1 = 0.0476, wR2 = 0.0774	
Extinction coefficient	n/a	
Largest diff. peak and hole	0.965 and -0.974 e $Å^{-3}$	

Table S4. Crystal data and structure refinement for compound **Ir-D2 (CCDC 2338502)**.

Identification code	emmlb230531sq	
Empirical formula	C91 H92 Cl14 F12 Ir2 N10 P2 S2, solvent 'C84 H78 Ir2 N10 S2, 2(F6 P), 7(CH2Cl2),solvent'	
Formula weight	2560.50	
Temperature	120(2) K	
Wavelength	0.71073 Å	
Crystal system, space group	Monoclinic, P 21/c	
Unit cell dimensions	*a* = 20.331(5) Å	α = 90°
	b = 17.476(4) Å	β = 92.474(7)°
	c = 16.089(4) Å	γ = 90°
Volume	5711(2) Å^3	
Z, Calculated density	2, 1.489 Mg/m^3	
Absorption coefficient	2.784 mm^{-1}	
F(000)	2540	
Crystal size	0.220 x 0.200 x 0.160 mm	
Theta range for data collection	1.964 to 28.224°	
Limiting indices	-26<=h<=26, -22<=k<=23, -21<=l<=21	
Reflections collected / unique	149962 / 13771 [R(int) = 0.0988]	
Completeness to theta = 25.242	100.0%	
Absorption correction	Semi-empirical from equivalents	
Max. and min. transmission	0.7456 and 0.5039	
Refinement method	Full-matrix least-squares on F^2	
Data / restraints / parameters	13771 / 0 / 613	
Goodness-of-fit on F^2 1.098		
Final R indices [I>2sigma(I)]	R1 = 0.0781, wR2 = 0.2059	
R indices (all data)	R1 = 0.1140, wR2 = 0.2393	
Extinction coefficient	n/a	
Largest diff. peak and hole	2.847 and -2.499 *e* Å^{-3}	

Table S5. Selected structural parameters of the experimental and theoretical structure of **Ir-D1**. Bond lengths are in [Å], angles and dihedral angles are in [°]. Theoretical results covers *meso*- and (Δ,Δ) stereoisomers, ground states and T_1 structures. *meso*-**Ir-D1** adopt a C_i symmetry and *ΔΔ*-**Ir-D1** a C_2 symmetry at ground state. See Figure S7 for atom numerotation. *Bq** is the barycenter of C_1 and C_1'.

Bond	**Exp**	**S_0 ΔΛ**	**T_1 ΔΛ**	**S_0 ΔΔ**	**T_1 ΔΔ**
Ir-N_1	2.122	2.172	2.193	2.17	2.197
Ir-N_2	2.165	2.197	2.208	2.20	2.207
Ir-N_3	2.053	2.070	2.068	2.07	2.074
Ir-N_4	2.047	2.071	2.071	2.07	2.065
Ir-C_{32}	2.005	2.017	1.991	2.02	1.993
Ir-C_{43}	2.008	2.016	1.987	2.02	1.989
Ir'-N_1'	2.122	2.172	2.171	2.17	2.184
Ir'-N_2'	2.165	2.197	2.192	2.20	2.190
Ir'-N_3'	2.053	2.070	2.068	2.07	2.065
Ir'-N_4'	2.047	2.071	2.070	2.07	2.074
Ir'-C_{32}'	2.005	2.017	2.019	2.02	2.019
Ir'-C_{43}'	2.008	2.016	2.018	2.02	2.015
Angle					
N_1-C_1-C_1'-N_1'	180.00	180.00	-179.57	178.82	176.63
N_1-C_2-C_3-N_2	-1.63	3.14	5.62	-3.70	5.12
N_1'-C_2'-C_3'-N_2'	1.63	-3.14	-1.37	-3.70	5.88
X-C_6-C_8-C_9	-37.80	-34.96	-29.51	36.54	33.70
X'-C_6'-C_8'-C_9'	37.80	34.96	38.08	36.54	-35.89
C_{11}-*Bq-C_{11}'**	177.86	180.00	177.56	168.80	160.04

Table S6. Selected structural parameters of the experimental and theoretical structure of **Ir-D2**. Bond lengths are in [Å], angles and dihedral angles are in [°]. Theoretical results covers *meso*- and (Δ,Δ) stereoisomers, ground states and T_1 structures. *meso*-**Ir-D2** adopt a C_i symmetry and *ΔΔ*-**Ir-D2** a C_2 symmetry at ground state. See Figure S7 for atom numerotation. *Bq** is the barycenter of C_{14} and C_{14}'.

Bond	**Exp**	**S_0 ΔΛ**	**T_1 ΔΛ**	**S_0 ΔΔ**	**T_1 ΔΔ**
Ir-N_1	2.149	2.177	2.198	2.176	2.179
Ir-N_2	2.170	2.186	2.206	2.189	2.179
Ir-N_3	2.050	2.070	2.070	2.073	2.071
Ir-N_4	2.049	2.072	2.073	2.070	2.070
Ir-C_{32}	2.021	2.017	1.985	2.017	2.018
Ir-C_{43}	2.024	2.017	1.989	2.017	2.020
Ir'-N_1'	2.149	2.177	2.179	2.176	2.202
Ir'-N_2'	2.170	2.186	2.183	2.189	2.204
Ir'-N_3'	2.050	2.070	2.068	2.070	2.073
Ir'-N_4'	2.049	2.072	2.072	2.073	2.070
Ir'-C_{32}'	2.021	2.017	2.018	2.017	1.985
Ir'-C_{43}'	2.024	2.017	2.019	2.017	1.989
Angle					
N_1-C_1-C_1'-N_1'	180.00	180.00	179.23	178.85	-179.85
N_1-C_2-C_3-N_2	-2.17	4.10	0.85	-2.58	3.78
N_1'-C_2'-C_3'-N_2'	2.17	-4.10	-5.33	-2.58	2.41
X-C_6-C_8-C_9	16.59	-16.83	-26.09	28.78	-19.23
X'-C_6'-C_8'-C_9'	-16.40	16.83	19.17	28.78	12.50
C_{11}-*Bq-C_{11}'**	180.00	180.00	167.07	167.65	176.10

Table S7. Selected structural parameters of the experimental and theoretical structure of **Ir-M1**. Bond lengths are in [Å], angles and dihedral angles are in [°]. Theoretical results covers ground states and T1 structures. See Figure S7 for atom numerotation. *Bq** is the barycenter of C_{14} and C_{14}'.

Bond	**Exp**	**S_0**	**T_1**
Ir-N_1	2.047	2.071	2.070
Ir-N_2	2.051	2.066	2.066
Ir-N_3	2.140	2.194	2.208
Ir-N_4	2.163	2.221	2.198
Ir-C_{32}	2.015	2.020	1.986
Ir-C_{43}	1.999	2.015	2.001
Angle			
N_1-C_2-C_3-N_2	0.60	1.043	2.00
X-C_6-C_8-C_9	47.70	29.38	28.88

Table S8. Selected structural parameters of the experimental and theoretical structure of **Ir-M2**. Bond lengths are in [Å], angles and dihedral angles are in [°]. Theoretical results covers ground states and T1 structures. See Figure S7 for atom numerotation. *Bq** is the barycenter of C_{14} and C_{14}'.

Bond	**Exp**	**S0**	**T1**
Ir-N_1	2.023	2.071	2.070
Ir-N_2	2.052	2.068	2.068
Ir-N_3	2.121	2.183	2.203
Ir-N_4	2.191	2.223	2.206
Ir-C_{32}	2.001	2.021	1.985
Ir-C_{43}	2.005	2.016	2.000
Angle			
N_1-C_2-C_3-N_2	0.18	1.924	2.30
X-C_6-C_8-C_9	28.78	17.85	-16.10

Table S9. Description of the main peaks of the absorption spectra of the complexes **Ir-M1**, **Ir-M2**, ***meso*-Ir-D1** and ***meso*-Ir-D2**.

Complex	**Singlet State**	**E** [eV]	**λ** (*f*) [nm]	**Transition character**
Ir-M1	S6	3.229	384 (0.9918)	LC
	S22	4.077	304 (0.2504)	$L_{ppy}C$
	S37	4.502	275 (0.2621)	$ML_{ppy}CT/L_{ppy}C$
Ir-M2	S5	3.069	404 (0.5184)	Mixed, involving the **L2** ligand
	S21	3.917	317 (0.1575)	Mixed
	S32	4.242	292 (0.1872)	$L_{ppy}C$
Ir-D1	S3	2.552	485 (1.0155)	MLCT/LC
	S8	2.795	444 (0.4090)	MLCT/LLCT
	S20	3.151	393 (0.2739)	centered on ppy
Ir-D2	S3	2.411	514 (1.4372)	LC
	S9	2.643	469 (0.5862)	MLCT/LLCT
	S23	3.193	388 (0.2646)	$L_{ppy}C/ML_{ppy}CT$

Table S10. Summary of the EL characteristics of the NIR LECs exhibiting EL peak wavelength >750 nm along with the corresponding reference.

Compound [a]	Driving mode	EL_{max} (nm)	L_{max} ($\mu W\ cm^{-2}$) [b]	$\eta_{ext,\ max}$ (%) [c]	$t_{1/2}$ (h) [d]	Ref.
Ru complex (mononuclear)	14 V	880	*ca.* 5.7	0.075	-	[53]
Ru complex (mononuclear)	6 V	900	*ca.* 2.5	0.006	-	[53]
Ru complex (mononuclear)	15 V	945	*ca.* 3.1	0.03	-	[53]
Ru complex (multinuclear)	5 V	780	*ca.* 30.8	0.013	-	[53]
Ru complex (multinuclear)	-	1040	-	-	-	[53]
Ru complex (multinuclear)	6 V	790	*ca.* 0.017	5.4×10^{-6}	*ca.* 0.025	[54]
Ir complex (mononuclear)	4 V	882	44.1	0.036	0.012	[25]
Ir complex (mononuclear)	4 V	790	56.9	0.05	0.003	[25]
Ir complex (mononuclear)	4 V	860 [e]	143	0.26	0.017	[20]
Copper complex (multinuclear)	I-V-L	*ca.* 755	-	-	-	[55]
Small molecule	2.5 V	805	8.19	1.49	>5	[56]
Small molecule	75 mA cm^{-2}	745, 810	134	0.121	>1.67	[57]
Small molecule	Pulsed current (current ramp) [f]	825	19	0.06	-	[58]
Small molecule	Pulsed current (7.5 mA) [g]	*ca.* 670/*ca.* 755	*ca.* 4.6	0.16	*ca.* 1.9	[59]
Small molecule	75 mA cm^{-2}	675/900	36	0.028	>24	[60]
Small molecule	Pulsed current (20 mA) [g]	656/765	65.9	0.014	0.2	[61]
Small molecule	Pulsed current (20 mA) [g]	722/778	82.8	0.03	0.81	[61]
Small molecule	Pulsed current (20 mA) [g]	*ca.* 737/*ca.* 790	55.7	0.022	1.1	[61]
Small molecule	Pulsed current (20 mA) [g]	*ca.* 656/*ca.* 778	48.2	0.01	0.92	[61]
Conjugated polymer	75 mA cm^{-2}	770	107	0.093	>20	[62]
Ir-D2	2.5 V 2.5 V 2.5 V	793 [h] 788 [i] 804 [j]	39.8 43.3 29.9	0.11 0.14 0.13	0.27 0.42 0.49	This work

[a] Category of the emissive material. [b] Maximal light output. [c] Maximal external quantum efficiency. [d] Time required for the light output of the device to decay from the maximum value to half of the maximum value. [e] Excimer emission. [f] Pulsed current mode (235 Hz, 50% duty cycle). [g] Pulsed driving scheme based on a block-wave at 1000 Hz and a duty cycle of 50% (average current). [h] Device thickness 107 nm. [i] Device thickness 156 nm. [j] Device thickness 205 nm.

Upon excited state geometry optimization, the degeneracy of the lowest singlet and triplet state is not lifted in the four complexes, and the energy difference between these states remains small. For all complexes the computed emission wavelength difference between S_1 and T_1 is smaller than 20 nm (Table 6). Upon these results a contribution of the singlet state to the emission may be fully excluded although no implication of the S_1 was observed experimentally. Inclusion of the SOC perturbation does not qualitatively modify the emission properties, with the four lowest states arising from the mixing of S_1 and T_1 still lying very close in energy (Table S11). The computed radiative rate constants are consistent with the experimental ones, with slightly greater values for the mononuclear than for the binuclear compounds (*cf.* Table 2 and Table S11). Again, it should be noticed that the properties of E_4, mainly generated by S_1, are very similar to those of E_1, E_2 and E_3 generated by the three components of T_1.

Table S11. Emission wavelengths computed for the four lowest SOC states at the T_1 geometry as well as oscillator strength, radiative rate constant and associated composition for complexes **Ir-M1**, **Ir-M2**, ***meso*-Ir-D1** and ***meso*-Ir-D2**. a) value averaged on the three substates contribution following a Boltzmann population of the states at 293 K (see Electronic Supplementary Information for details).

complex	SOC state	λ_{em} [nm]	Oscillator strength	$10^5\ k_r$ k_r	$10^5\ k_r$ (average)[a]	% contributing state
Ir-M1	E_1	706	$1.21\ 10^{-4}$	0.16	5.8	89% T_1, 4% T_2, 4% T_3, 2% T_4
	E_2	705	$6.19\ 10^{-3}$	8.31		88% T_1, 3% T_3, 3% S_1, 2% S_2
	E_3	701	$8.58\ 10^{-3}$	11.7		93% T_1, 2% T_4, 1% S_3
	E_4	695	$1.31\ 10^{-3}$	1.81		85% S_1, 4% T_2, 4% T_3, 3% T_1
Ir-M2	E_1	779	$1.27\ 10^{-4}$	0.14	5.2	91% T_1, 3% T_2, 3% T_3, 2% T_4
	E_2	777	$6.04\ 10^{-3}$	6.67		91% T_1, 3% T_3, 2% S_2
	E_3	773	$1.03\ 10^{-2}$	11.5		93% T_1, 2% T_4, 1% S_1
	E_4	765	$5.39\ 10^{-4}$	0.62		87% S_1, 3% T_2, 2% T_4, 2% T_1
Ir-D1	E_1	830	$1.18\ 10^{-5}$	0.01	3.6	93% T_1, 3% T_4, 2% T_3
	E_2	829	$9.23\ 10^{-3}$	8.95		92% T_1, 3% T_4, 2% S_1
	E_3	827	$1.99\ 10^{-3}$	1.94		93% T_1, 2% S_1, 1% S_{11}
	E_4	817	$5.25\ 10^{-3}$	5.24		88% S_1, 4% T_1, 3% T_4, 1% T_3
Ir-D2	E_1	925	$1.23\ 10^{-5}$	0.009	3.2	94% T_1, 2% T_4, 1% T_8
	E_2	924	$9.52\ 10^{-3}$	7.44		94% T_1, 2% T_2, 1% S_7
	E_3	921	$3.14\ 10^{-3}$	2.47		92% T_1, 4% S_1, 1% S_{10}
	E_4	910	$1.46\ 10^{-3}$	1.17		89% S_1, 4% T_1, 2% T_4, 1% T_8

Table S12. Vertical excitations calculated for *meso*-**Ir-D1** and *meso*-**Ir-D2**.

meso-**Ir-D1**			
State	**E (eV)**	**λ (nm)**	**f**
S1	1.895	654	0.000E+00
S2	1.914	648	4.055E-03
S3	2.552	486	1.015E+00
S4	2.623	473	0.000E+00
S5	2.632	471	1.031E-01
S6	2.666	465	0.000E+00
S7	2.770	448	2.362E-01
S8	2.795	444	4.090E-01
S9	2.800	443	0.000E+00
S10	2.826	439	3.688E-01
S11	2.850	435	0.000E+00
S12	2.924	424	0.000E+00
S13	2.935	422	7.402E-02
S14	2.957	419	0.000E+00
S15	2.957	419	1.221E-02

meso-**Ir-D2**			
State	**E (eV)**	**λ (nm)**	**f**
S1	1.747	710	0.000E+00
S2	1.765	702	3.468E-03
S3	2.411	514	1.437E+00
S4	2.464	503	0.000E+00
S5	2.470	502	8.810E-03
S6	2.536	489	1.453E-02
S7	2.539	488	0.000E+00
S8	2.565	483	0.000E+00
S9	2.643	469	5.862E-01
S10	2.710	457	4.197E-01
S11	2.730	454	0.000E+00
S12	2.761	449	0.000E+00
S13	2.766	448	3.190E-02
S14	2.790	444	0.000E+00
S15	2.797	443	4.610E-02

S16	3.073	403	2.732E-02	S16	2.913	426	3.485E-02
S17	3.075	403	0.000E+00	S17	2.924	424	0.000E+00
S18	3.137	395	0.000E+00	S18	3.038	408	0.000E+00
S19	3.148	394	0.000E+00	S19	3.046	407	3.222E-02
S20	3.151	393	2.739E-01	S20	3.055	406	0.000E+00
S21	3.233	383	6.970E-03	S21	3.173	391	0.000E+00
S22	3.236	383	0.000E+00	S22	3.191	389	0.000E+00
S23	3.436	361	0.000E+00	S23	3.193	388	2.646E-01
S24	3.460	358	0.000E+00	S24	3.238	383	3.672E-02
S25	3.461	358	9.145E-03	S25	3.270	379	0.000E+00
T1	1.881	659		T1	1.730	717	
T2	1.891	656		T2	1.741	712	
T3	2.127	583		T3	1.987	624	
T4	2.541	488		T4	2.374	522	
T5	2.546	487		T5	2.417	513	
T6	2.567	483		T6	2.444	507	
T7	2.651	468		T7	2.495	497	
T8	2.712	457		T8	2.529	490	
T9	2.715	457		T9	2.531	490	
T10	2.760	449		T10	2.544	487	
T11	2.782	446		T11	2.583	480	
T12	2.807	442		T12	2.613	474	
T13	2.863	433		T13	2.622	473	
T14	2.864	433		T14	2.665	465	
T15	2.882	430		T15	2.756	450	
T16	2.884	430		T16	2.783	446	
T17	2.917	425		T17	2.888	429	
T18	2.936	422		T18	2.892	429	
T19	2.936	422		T19	2.897	428	
T20	2.960	419		T20	2.925	424	
T21	3.057	406		T21	2.946	421	
T22	3.083	402		T22	2.946	421	
T23	3.150	394		T23	2.963	418	
T24	3.158	393		T24	3.027	410	
T25	3.363	369		T25	3.076	403	
E1	1.817	682	0.000E+00	E1	1.671	742	0.000E+00
E2	1.818	682	0.000E+00	E2	1.673	741	0.000E+00
E3	1.822	681	5.577E-05	E3	1.678	739	0.000E+00
E4	1.823	680	0.000E+00	E4	1.678	739	3.659E-05
E5	1.825	679	2.469E-02	E5	1.681	737	2.380E-02
E6	1.829	678	7.967E-03	E6	1.686	735	1.096E-02
E7	1.830	677	0.000E+00	E7	1.688	735	0.000E+00
E8	1.846	672	9.892E-03	E8	1.703	728	8.803E-03
E9	2.134	581	2.748E-05	E9	1.992	622	2.164E-05
E10	2.134	581	9.316E-04	E10	1.993	622	4.390E-04
E11	2.134	581	1.689E-03	E11	1.993	622	1.444E-03
E12	2.466	503	3.907E-01	E12	2.328	532	0.000E+00
E13	2.467	502	0.000E+00	E13	2.328	532	0.000E+00
E14	2.468	502	0.000E+00	E14	2.343	529	0.000E+00
E15	2.490	498	0.000E+00	E15	2.344	529	5.931E-01

E16	2.496	497	1.953E-03	E16	2.368	523	1.728E-03
E17	2.496	497	8.055E-03	E17	2.369	523	4.907E-03
E18	2.519	492	0.000E+00	E18	2.401	516	0.000E+00
E19	2.571	482	5.830E-02	E19	2.427	511	2.086E-01
E20	2.620	473	5.389E-01	E20	2.453	506	0.000E+00
E21	2.631	471	0.000E+00	E21	2.453	505	0.000E+00
E22	2.631	471	0.000E+00	E22	2.462	504	0.000E+00
E23	2.646	468	0.000E+00	E23	2.462	503	4.547E-01
E24	2.672	464	1.227E-03	E24	2.485	499	2.034E-03
E25	2.673	464	2.248E-03	E25	2.490	498	5.810E-04
E26	2.678	463	1.207E-01	E26	2.502	495	6.634E-02
E27	2.691	461	0.000E+00	E27	2.511	494	0.000E+00
E28	2.703	459	8.117E-02	E28	2.512	494	1.073E-01
E29	2.719	456	0.000E+00	E29	2.519	492	0.000E+00
E30	2.720	456	0.000E+00	E30	2.522	492	0.000E+00
E31	2.726	455	0.000E+00	E31	2.533	489	0.000E+00
E32	2.767	448	1.229E-03	E32	2.542	488	5.831E-03
E33	2.768	448	2.004E-03	E33	2.546	487	1.687E-03
E34	2.774	447	0.000E+00	E34	2.553	486	4.395E-02
E35	2.779	446	0.000E+00	E35	2.559	484	0.000E+00
E36	2.782	446	0.000E+00	E36	2.560	484	0.000E+00
E37	2.782	446	1.357E-02	E37	2.568	483	0.000E+00
E38	2.789	445	1.614E-01	E38	2.571	482	0.000E+00
E39	2.793	444	2.709E-03	E39	2.575	481	1.078E-01
E40	2.796	443	1.271E-01	E40	2.615	474	7.296E-05
E41	2.800	443	0.000E+00	E41	2.615	474	2.683E-05
E42	2.820	440	0.000E+00	E42	2.616	474	0.000E+00
E43	2.823	439	0.000E+00	E43	2.617	474	0.000E+00
E44	2.824	439	2.956E-01	E44	2.617	474	0.000E+00
E45	2.828	438	0.000E+00	E45	2.619	473	1.079E-02
E46	2.863	433	6.124E-03	E46	2.654	467	2.731E-04
E47	2.863	433	4.384E-05	E47	2.654	467	7.819E-05
E48	2.863	433	1.946E-04	E48	2.686	462	4.406E-01
E49	2.864	433	0.000E+00	E49	2.693	460	0.000E+00
E50	2.864	433	0.000E+00	E50	2.693	460	0.000E+00
E51	2.864	433	0.000E+00	E51	2.698	459	0.000E+00
E52	2.869	432	0.000E+00	E52	2.723	455	1.431E-01
E53	2.869	432	1.263E-01	E53	2.730	454	0.000E+00
E54	2.881	430	0.000E+00	E54	2.770	448	3.695E-02
E55	2.883	430	2.495E-04	E55	2.772	447	0.000E+00
E56	2.883	430	0.000E+00	E56	2.778	446	8.089E-05
E57	2.883	430	8.277E-04	E57	2.778	446	5.662E-03
E58	2.884	430	0.000E+00	E58	2.810	441	1.453E-01
E59	2.886	430	2.628E-02	E59	2.811	441	0.000E+00
E60	2.927	424	1.423E-04	E60	2.822	439	0.000E+00
E61	2.927	424	4.130E-03	E61	2.822	439	0.000E+00
E62	2.935	422	0.000E+00	E62	2.832	438	9.446E-02
E63	2.936	422	9.579E-04	E63	2.849	435	0.000E+00
E64	2.937	422	0.000E+00	E64	2.889	429	5.218E-04
E65	2.938	422	1.617E-03	E65	2.889	429	1.783E-03

E66	2.938	422	0.000E+00	E66	2.890	429	3.879E-04
E67	2.938	422	1.024E-03	E67	2.890	429	0.000E+00
E68	2.943	421	0.000E+00	E68	2.890	429	0.000E+00
E69	2.948	421	7.125E-02	E69	2.892	429	0.000E+00
E70	2.953	420	9.672E-02	E70	2.901	427	1.472E-04
E71	2.957	419	0.000E+00	E71	2.901	427	4.683E-03
E72	2.960	419	2.129E-02	E72	2.903	427	1.578E-02
E73	2.983	416	0.000E+00	E73	2.926	424	3.467E-02
E74	2.983	416	0.000E+00	E74	2.929	423	0.000E+00
E75	2.997	414	0.000E+00	E75	2.933	423	0.000E+00
E76	3.062	405	1.173E-04	E76	2.933	423	0.000E+00
E77	3.063	405	2.168E-03	E77	2.934	422	0.000E+00
E78	3.065	405	1.149E-02	E78	2.945	421	0.000E+00
E79	3.079	403	0.000E+00	E79	2.946	421	5.127E-04
E80	3.080	402	2.688E-02	E80	2.947	421	0.000E+00
E81	3.089	401	0.000E+00	E81	2.947	421	9.714E-05
E82	3.090	401	0.000E+00	E82	2.947	421	0.000E+00
E83	3.091	401	0.000E+00	E83	2.948	421	6.307E-04
E84	3.142	395	0.000E+00	E84	2.969	418	0.000E+00
E85	3.150	394	0.000E+00	E85	2.970	417	0.000E+00
E86	3.151	393	1.233E-01	E86	2.970	417	0.000E+00
E87	3.152	393	2.905E-04	E87	3.024	410	7.150E-03
E88	3.152	393	9.944E-03	E88	3.030	409	1.621E-04
E89	3.153	393	1.405E-01	E89	3.030	409	2.336E-03
E90	3.167	391	0.000E+00	E90	3.039	408	0.000E+00
E91	3.167	391	0.000E+00	E91	3.053	406	2.542E-02
E92	3.169	391	0.000E+00	E92	3.069	404	0.000E+00
E93	3.229	384	0.000E+00	E93	3.076	403	0.000E+00
E94	3.235	383	6.978E-03	E94	3.077	403	0.000E+00
E95	3.366	368	0.000E+00	E95	3.078	403	0.000E+00
E96	3.369	368	0.000E+00	E96	3.184	389	0.000E+00
E97	3.374	367	0.000E+00	E97	3.193	388	0.000E+00
E98	3.448	360	0.000E+00	E98	3.194	388	2.641E-01
E99	3.462	358	9.136E-03	E99	3.246	382	3.635E-02
E100	3.465	358	0.000E+00	E100	3.276	378	0.000E+00

Table S13. Vertical excitations calculated for **Ir-M1** and **Ir-M2**.

Ir-M1				Ir-M2			
State	**E (eV)**	**λ (nm)**	**f**	**State**	**E (eV)**	**λ (nm)**	**f**
S1	2.294	540	1.385E-03	S1	2.101	590	9.396E-04
S2	2.913	426	1.161E-01	S2	2.734	454	1.160E-01
S3	3.014	411	7.058E-02	S3	2.833	438	2.224E-02
S4	3.131	396	1.214E-01	S4	2.983	416	5.005E-01
S5	3.155	393	1.856E-01	S5	3.069	404	5.184E-01
S6	3.229	384	9.918E-01	S6	3.079	403	3.568E-01
S7	3.258	381	6.921E-02	S7	3.161	392	7.967E-02
S8	3.378	367	4.748E-02	S8	3.166	392	1.200E-01
S9	3.447	360	1.995E-02	S9	3.279	378	3.699E-03

S10	3.505	354	1.061E-02
S11	3.569	347	1.431E-02
S12	3.741	331	7.651E-03
S13	3.747	331	7.182E-02
S14	3.760	330	3.303E-02
S15	3.828	324	3.826E-02
S16	3.846	322	4.458E-03
S17	3.892	319	7.935E-02
S18	3.932	315	1.424E-01
S19	3.947	314	3.549E-02
S20	4.024	308	2.903E-02
S21	4.058	306	1.314E-01
S22	4.077	304	2.504E-01
S23	4.097	303	8.652E-02
S24	4.131	300	5.700E-02
S25	4.216	294	1.374E-01
S26	4.243	292	8.088E-02
S27	4.259	291	5.195E-02
S28	4.273	290	2.844E-02
S29	4.290	289	8.011E-02
S30	4.306	288	3.250E-02
S31	4.327	287	2.998E-02
S32	4.355	285	8.339E-03
S33	4.374	283	6.037E-02
S34	4.401	282	1.203E-02
S35	4.406	281	1.425E-02
S36	4.463	278	4.849E-02
S37	4.502	275	2.621E-01
S38	4.515	275	6.844E-02
S39	4.529	274	4.701E-03
S40	4.568	271	2.666E-02
T1	2.269	546	
T2	2.535	489	
T3	2.790	444	
T4	2.872	432	
T5	2.934	423	
T6	2.939	422	
T7	3.084	402	
T8	3.272	379	
T9	3.352	370	
T10	3.365	368	
T11	3.369	368	
T12	3.382	367	
T13	3.398	365	
T14	3.426	362	
T15	3.518	352	
T16	3.563	348	
T17	3.601	344	
T18	3.623	342	
T19	3.655	339	
T20	3.677	337	
T21	3.760	330	

S10	3.311	374	1.423E-02
S11	3.324	373	4.389E-02
S12	3.566	348	3.805E-02
S13	3.684	337	2.437E-02
S14	3.754	330	3.146E-02
S15	3.764	329	5.254E-02
S16	3.779	328	2.513E-02
S17	3.793	327	4.259E-02
S18	3.849	322	9.678E-02
S19	3.886	319	3.084E-02
S20	3.894	318	4.567E-02
S21	3.917	317	1.575E-01
S22	3.933	315	1.583E-02
S23	3.949	314	3.543E-02
S24	3.993	311	6.062E-02
S25	4.081	304	1.288E-01
S26	4.119	301	1.177E-01
S27	4.122	301	1.223E-02
S28	4.126	300	1.212E-01
S29	4.167	298	1.158E-02
S30	4.175	297	5.050E-02
S31	4.220	294	9.113E-03
S32	4.242	292	1.872E-01
S33	4.276	290	6.790E-02
S34	4.285	289	5.592E-02
S35	4.334	286	1.229E-02
S36	4.365	284	5.603E-03
S37	4.398	282	5.549E-02
S38	4.413	281	2.097E-03
S39	4.423	280	2.376E-02
S40	4.440	279	1.133E-02
T1	2.073	598	
T2	2.361	525	
T3	2.641	470	
T4	2.739	453	
T5	2.876	431	
T6	2.896	428	
T7	2.949	420	
T8	3.064	405	
T9	3.077	403	
T10	3.099	400	
T11	3.191	389	
T12	3.228	384	
T13	3.298	376	
T14	3.341	371	
T15	3.391	366	
T16	3.403	364	
T17	3.485	356	
T18	3.539	350	
T19	3.621	342	
T20	3.664	338	
T21	3.679	337	

T22	3.788	327		T22	3.705	335	
T23	3.838	323		T23	3.750	331	
T24	3.904	318		T24	3.804	326	
T25	3.961	313		T25	3.842	323	
T26	4.021	308		T26	3.843	323	
T27	4.048	306		T27	3.874	320	
T28	4.087	303		T28	3.965	313	
T29	4.123	301		T29	4.028	308	
T30	4.163	298		T30	4.040	307	
T31	4.192	296		T31	4.081	304	
T32	4.211	294		T32	4.116	301	
T33	4.227	293		T33	4.123	301	
T34	4.233	293		T34	4.148	299	
T35	4.250	292		T35	4.157	298	
T36	4.259	291		T36	4.194	296	
T37	4.271	290		T37	4.195	296	
T38	4.283	289		T38	4.214	294	
T39	4.293	289		T39	4.222	294	
T40	4.304	288		T40	4.232	293	
E1	2.176	570	5.972E-05	E1	1.987	624	1.659E-04
E2	2.181	569	5.910E-03	E2	1.991	623	6.341E-03
E3	2.191	566	7.059E-03	E3	2.002	619	9.622E-03
E4	2.199	564	1.849E-03	E4	2.013	616	1.587E-03
E5	2.545	487	1.525E-04	E5	2.367	524	1.333E-04
E6	2.546	487	5.654E-04	E6	2.369	523	1.850E-04
E7	2.547	487	1.992E-04	E7	2.369	523	9.179E-04
E8	2.755	450	2.473E-02	E8	2.599	477	2.856E-02
E9	2.771	447	9.278E-04	E9	2.600	477	8.661E-04
E10	2.773	447	7.208E-04	E10	2.602	477	1.957E-03
E11	2.826	439	2.415E-04	E11	2.676	463	3.526E-02
E12	2.828	438	1.048E-03	E12	2.798	443	6.252E-04
E13	2.831	438	1.213E-03	E13	2.802	442	3.190E-03
E14	2.874	431	2.628E-02	E14	2.831	438	5.306E-02
E15	2.893	428	1.592E-03	E15	2.845	436	1.962E-02
E16	2.898	428	2.121E-03	E16	2.855	434	2.160E-03
E17	2.900	428	1.733E-03	E17	2.857	434	1.727E-03
E18	2.988	415	7.147E-04	E18	2.862	433	8.791E-03
E19	2.989	415	1.652E-03	E19	2.883	430	4.185E-03
E20	2.996	414	7.744E-02	E20	2.884	430	3.623E-03
E21	3.037	408	9.603E-02	E21	2.888	429	1.822E-02
E22	3.056	406	5.938E-02	E22	2.910	426	2.478E-03
E23	3.088	401	6.068E-04	E23	2.912	426	4.645E-03
E24	3.088	401	6.103E-03	E24	2.914	425	2.209E-03
E25	3.089	401	1.361E-02	E25	2.989	415	3.908E-01
E26	3.134	396	1.093E-01	E26	3.007	412	3.989E-01
E27	3.187	389	2.699E-01	E27	3.014	411	4.841E-03
E28	3.241	383	7.418E-01	E28	3.017	411	1.449E-02
E29	3.279	378	3.642E-04	E29	3.019	411	1.229E-02
E30	3.280	378	3.246E-02	E30	3.064	405	2.042E-03
E31	3.280	378	4.302E-03	E31	3.064	405	8.155E-05
E32	3.309	375	5.357E-04	E32	3.065	405	7.515E-04
E33	3.312	374	2.869E-03	E33	3.083	402	2.645E-01

E34	3.320	373	3.848E-03	E34	3.084	402	1.459E-01
E35	3.336	372	2.022E-03	E35	3.103	400	2.733E-04
E36	3.338	371	1.829E-03	E36	3.104	399	2.296E-02
E37	3.350	370	2.316E-03	E37	3.106	399	4.753E-02
E38	3.355	370	4.182E-03	E38	3.167	391	6.893E-02
E39	3.355	370	3.318E-03	E39	3.199	388	4.612E-03
E40	3.357	369	1.953E-03	E40	3.199	388	2.078E-03
E41	3.359	369	3.691E-03	E41	3.201	387	1.340E-02
E42	3.362	369	1.048E-02	E42	3.214	386	1.031E-02
E43	3.369	368	2.937E-03	E43	3.237	383	2.359E-03
E44	3.371	368	4.651E-04	E44	3.239	383	2.825E-03
E45	3.371	368	3.658E-04	E45	3.246	382	2.959E-02
E46	3.374	367	6.238E-03	E46	3.285	377	5.772E-03
E47	3.386	366	3.857E-02	E47	3.303	375	2.766E-03
E48	3.402	364	1.186E-02	E48	3.304	375	2.019E-03
E49	3.439	361	1.633E-03	E49	3.305	375	3.448E-03
E50	3.439	360	5.949E-04	E50	3.322	373	3.881E-02
E51	3.444	360	1.066E-02	E51	3.344	371	9.286E-04
E52	3.507	353	8.126E-03	E52	3.346	370	3.609E-03
E53	3.515	353	3.265E-03	E53	3.349	370	6.661E-03
E54	3.518	352	1.211E-03	E54	3.358	369	1.139E-03
E55	3.521	352	2.114E-03	E55	3.360	369	2.647E-03
E56	3.531	351	1.775E-03	E56	3.367	368	1.906E-03
E57	3.533	351	2.030E-03	E57	3.372	368	1.651E-03
E58	3.535	351	1.436E-03	E58	3.386	366	6.700E-03
E59	3.567	348	1.230E-02	E59	3.410	364	5.175E-03
E60	3.569	347	1.420E-02	E60	3.485	356	3.483E-04
E61	3.582	346	4.440E-03	E61	3.486	356	1.696E-04
E62	3.585	346	1.500E-03	E62	3.486	356	2.429E-05
E63	3.597	345	6.968E-03	E63	3.522	352	1.434E-03
E64	3.603	344	2.218E-03	E64	3.528	351	1.107E-04
E65	3.610	343	3.383E-03	E65	3.528	351	1.085E-03
E66	3.638	341	8.006E-03	E66	3.573	347	3.695E-02
E67	3.645	340	2.446E-03	E67	3.595	345	9.396E-03
E68	3.647	340	3.711E-03	E68	3.600	344	2.024E-02
E69	3.668	338	5.483E-03	E69	3.603	344	5.592E-03
E70	3.673	338	1.303E-03	E70	3.617	343	5.342E-03
E71	3.675	337	4.415E-04	E71	3.622	342	1.052E-02
E72	3.699	335	3.638E-02	E72	3.628	342	7.471E-03
E73	3.711	334	9.149E-03	E73	3.639	341	3.417E-03
E74	3.749	331	1.768E-02	E74	3.644	340	4.284E-03
E75	3.765	329	3.463E-02	E75	3.651	340	3.515E-03
E76	3.819	325	2.529E-03	E76	3.672	338	1.117E-02
E77	3.823	324	5.366E-04	E77	3.687	336	1.485E-02
E78	3.829	324	1.156E-03	E78	3.697	335	2.262E-03
E79	3.833	323	1.671E-03	E79	3.704	335	4.269E-03
E80	3.840	323	6.176E-03	E80	3.746	331	2.884E-02
E81	3.843	323	5.238E-03	E81	3.753	330	1.248E-02
E82	3.860	321	1.722E-02	E82	3.775	328	2.331E-02
E83	3.875	320	2.731E-03	E83	3.784	328	1.849E-02
E84	3.878	320	1.665E-03	E84	3.796	327	6.401E-03
E85	3.895	318	2.066E-02	E85	3.799	326	8.992E-03

E86	3.898	318	1.956E-02	E86	3.802	326	2.619E-02
E87	3.914	317	5.433E-02	E87	3.814	325	1.412E-02
E88	3.926	316	1.925E-03	E88	3.837	323	1.693E-03
E89	3.927	316	4.731E-03	E89	3.841	323	3.532E-03
E90	3.939	315	4.468E-02	E90	3.847	322	4.204E-02
E91	3.942	315	1.370E-02	E91	3.853	322	3.319E-02
E92	3.943	314	3.334E-02	E92	3.868	321	2.063E-02
E93	3.973	312	4.508E-02	E93	3.873	320	2.414E-03
E94	3.979	312	3.879E-02	E94	3.882	319	6.917E-03
E95	3.994	310	3.429E-02	E95	3.889	319	2.574E-02
E96	4.011	309	3.080E-03	E96	3.897	318	1.579E-02
E97	4.020	308	2.241E-03	E97	3.898	318	5.528E-03
E98	4.034	307	7.974E-03	E98	3.904	318	2.721E-02
E99	4.039	307	3.808E-03	E99	3.921	316	3.722E-03
E100	4.047	306	9.851E-03	E100	3.924	316	5.317E-03
E101	4.052	306	1.230E-02	E101	3.938	315	1.087E-02
E102	4.076	304	6.547E-02	E102	3.942	314	4.256E-02
E103	4.100	302	1.584E-01	E103	3.959	313	7.315E-02
E104	4.122	301	1.048E-02	E104	3.976	312	3.569E-02
E105	4.123	301	1.401E-03	E105	4.004	310	2.682E-03
E106	4.128	300	5.249E-02	E106	4.006	310	2.547E-03
E107	4.131	300	3.634E-02	E107	4.014	309	3.196E-02
E108	4.137	300	5.725E-02	E108	4.027	308	1.927E-02
E109	4.150	299	1.841E-03	E109	4.034	307	1.055E-03
E110	4.151	299	5.168E-03	E110	4.035	307	5.469E-04
E111	4.155	298	8.881E-03	E111	4.038	307	6.243E-03
E112	4.162	298	8.023E-03	E112	4.048	306	9.837E-03
E113	4.167	298	1.618E-02	E113	4.050	306	1.613E-03
E114	4.169	297	2.336E-02	E114	4.059	305	3.482E-02
E115	4.187	296	1.212E-03	E115	4.082	304	2.758E-03
E116	4.191	296	5.405E-03	E116	4.084	304	3.654E-03
E117	4.195	296	4.728E-03	E117	4.086	303	1.449E-03
E118	4.206	295	1.290E-02	E118	4.110	302	6.077E-03
E119	4.213	294	9.975E-03	E119	4.111	302	9.018E-03
E120	4.215	294	1.177E-03	E120	4.111	302	2.601E-03
E121	4.216	294	7.028E-04	E121	4.114	301	6.430E-02
E122	4.218	294	4.724E-03	E122	4.121	301	1.470E-02
E123	4.221	294	2.824E-02	E123	4.126	301	1.638E-02
E124	4.230	293	6.886E-03	E124	4.128	300	1.498E-02
E125	4.231	293	2.576E-02	E125	4.130	300	7.345E-03
E126	4.234	293	9.927E-04	E126	4.140	300	6.739E-02
E127	4.236	293	1.480E-02	E127	4.146	299	4.860E-02
E128	4.237	293	3.410E-02	E128	4.153	299	1.643E-03
E129	4.245	292	4.267E-03	E129	4.154	298	3.140E-03
E130	4.250	292	1.334E-02	E130	4.160	298	4.098E-02
E131	4.254	291	3.939E-02	E131	4.163	298	8.615E-03
E132	4.255	291	2.852E-02	E132	4.165	298	7.647E-03
E133	4.264	291	3.012E-03	E133	4.165	298	4.378E-03
E134	4.264	291	6.316E-03	E134	4.172	297	1.318E-02
E135	4.267	291	2.301E-03	E135	4.188	296	1.676E-02
E136	4.274	290	3.146E-02	E136	4.193	296	3.772E-04
E137	4.285	289	8.648E-03	E137	4.195	296	1.185E-03

E138	4.288	289	5.489E-03	E138	4.197	295	1.180E-03
E139	4.291	289	2.023E-02	E139	4.198	295	1.649E-03
E140	4.295	289	7.049E-03	E140	4.199	295	5.007E-03
E141	4.297	289	2.394E-03	E141	4.207	295	2.643E-02
E142	4.299	288	7.636E-03	E142	4.212	294	6.211E-04
E143	4.303	288	1.599E-02	E143	4.217	294	2.928E-03
E144	4.308	288	4.349E-02	E144	4.217	294	7.087E-04
E145	4.320	287	1.683E-02	E145	4.223	294	1.358E-03
E146	4.328	286	1.011E-02	E146	4.224	293	1.228E-02
E147	4.332	286	1.001E-03	E147	4.228	293	1.319E-02
E148	4.334	286	2.332E-02	E148	4.229	293	8.418E-04
E149	4.348	285	2.425E-02	E149	4.244	292	1.477E-02
E150	4.355	285	1.669E-03	E150	4.248	292	9.467E-03
E151	4.357	285	8.260E-04	E151	4.250	292	3.735E-02
E152	4.368	284	8.693E-03	E152	4.260	291	1.161E-01
E153	4.397	282	4.145E-02	E153	4.286	289	6.536E-02
E154	4.405	281	1.216E-02	E154	4.297	289	5.053E-02
E155	4.470	277	4.251E-02	E155	4.342	286	1.244E-02
E156	4.516	275	6.012E-02	E156	4.387	283	5.314E-03
E157	4.523	274	1.010E-01	E157	4.410	281	5.193E-02
E158	4.528	274	1.444E-01	E158	4.428	280	2.391E-03
E159	4.542	273	3.614E-02	E159	4.438	279	2.482E-02
E160	4.570	271	2.701E-02	E160	4.442	279	1.130E-02

References

[S1] A. Jouaiti, L. Ballerini, H. Shen, R. Viel, F. Polo, N. Kyritsakas, S. Haacke, Y. Huang, C. Lu, C. Gourlaouen, H. Su, M. Mauro, *Angew. Chem. Int. Ed*. 2023, **62***,* e202305569.

[S2] G. A. Crosby, J. N. Demas, *J. Am. Chem. Soc.* 1970, **92**, 7262.

[S3] H. Ishida, S. Tobita, Y. Hasegawa, R. Katoh, K. Nozaki, *Coord. Chem. Rev.* 2010, **254**, 2449.

[S4] J. R. Lakowicz, in *Principles of Fluorescence Spectroscopy*, 3rd Ed., Springer, New York, 2006.

[S5] S. Antonello, M. Musumeci, D. D. M. Wayner, F. Maran, *J. Am. Chem. Soc.* 1997, **119**, 9541.

[S6] A. Belèn Meneses, S. Antonello, M. C. Arévalo, F. Maran, *Electroanalysis* 2006, **18**, 363.

[S7] P. J. Stephens, F. J. Devlin, C. F. Chabalowski, M. J. Frisch, *J. Phys. Chem.* 1994, **98**, 11623.

[S8] E. Van Lenthe, R. Van Leeuwen, E. J. Baerends, J. G. Snijders, C. Nieuwpoort, R. Broer, P. J. C. Aerts, P. S. Bagus, *Int. J. Quantum Chem.* 1996, **5**7, 281.

[S9] F. Wang, T. Ziegler, *J. Chem. Phys.* 2005*,* **123**, 154102.

[S10] F. Wang, T. Ziegler, E. van Lenthe, S. van Gisbergen, E. J. Baerends, *J. Chem. Phys*. 2005, **122**, 204103.

[S11] A. Klamt, *J. Phys. Chem.* 1995, **99,** 2224.

[S12] S. Grimme, J. Antony, S. Ehrlich, H. Krieg, *J. Chem. Phys*. 2010, **132**, 154104.

[S13] M. J. G. Peach, D. J. Tozer, *J. Phys. Chem A* 2012, **116**, 9783.

[S14] F. Plasser, *J. Chem. Phys*. 2020, **152**, 084108.

[S15] T. D. Goddard, C. C. Huang, E. C. Meng, E. F. Pettersen, G. S. Couch, J. H. Morris, T. E. Ferrin, *Protein Sci*. 2018, **27**, 14.

[S16] M86-EXX278V1 APEX4 User Manual", Bruker Corporation, 2021.

[S17] G. M. Sheldrick, *Acta Cryst*. 2015, **A71**, 3-8.

[S18] G. M. Sheldrick, *Acta Cryst*. 2015, **C71**, 3-8.

[S19] M86-EXX229V1 APEX3 User Manual", Bruker AXS Inc., Madison, USA, 2016.

[S20] A. L. Spek, *J. Appl. Crystallogr*. 2003, **36**, 7.